A Numerical Study of Factors Affecting Fracture Fluid Cleanup and Produced Gas/Water in Marcellus Shale (Part II)

Maxian B. Seales, SPE, The Pennsylvania State University; **Robert Dilmore,** National Energy Technology Laboratory; **Turgay Ertekin,** SPE, and **John Yilin Wang,** SPE, The Pennsylvania State University

Summary

Horizontal wells combined with successful multi-stage hydraulic fracture treatments are currently the most established method for effectively stimulating and enabling economic development of gas bearing organic-rich shale formations. Fracture cleanup in the Stimulated Reservoir Volume (SRV) is critical to stimulation effectiveness and long-term well performance. However, fluid cleanup is often hampered by formation damage, and post-fracture well performance frequently falls below expectations. A systematic study of the factors that hinder fracture fluid cleanup in shale formations can help optimize fracture treatments and better quantify long term volumes of produced water and gas.

Fracture fluid cleanup is a complex process influenced by multi-phase flow through porous media (relative permeability hysteresis, capillary pressure etc.), reservoir rock and fluid properties, fracture fluid properties, proppant placement, fracture treatment parameters, and subsequent flowback and field operations. Changing SRV and fracture conductivity as production progresses further adds to the complexity of this problem. Numerical simulation is the best, and most practical approach to investigate such a complicated blend of mechanisms, parameters, their interactions, and subsequent impact on fracture fluid cleanup and well deliverability.

In this paper, a 3-dimensional, 2-phase, dual-porosity model was used to investigate the impact of multiphase flow, proppant crushing, proppant diagenesis, shut-in time, reservoir rock compaction, gas slippage, and gas desorption on fracture fluid cleanup, and well performance in Marcellus shale. The research findings have shed light on the factors that substantially constrains efficient fracture fluid cleanup in gas shales, and provided guidelines for improved fracture treatment designs and water management.

Keywords: Shale gas, dual-porosity modeling, fracture fluid cleanup, Marcellus shale

Introduction

Gas shales, due to their ultralow permeability ($\approx 0.0001mD$), are incapable of producing economically feasible rates of gas or oil without effective stimulation, such as hydraulic fracturing. A fracture treatment starts with the injection of a pad fluid which breaks down the formation, creating new hydraulic fractures and/or stimulating pre-existing natural fractures. This process is followed by the injection of a proppant-laden slurry; the proppant props open the created fractures and maintain conductive paths to fluid flow for decades.

All hydraulic fracturing treatments require a post-stimulation flow period (cleanup) that returns the fracture fluid to the surface, and prepares the well for long-term production. However the reservoir typically captures a percentage of the injected fluid, which may later hinder oil and gas flow. Accordingly, the percentage of fracture fluid recovered is one of the key indicators of fracture treatment success or failure. The EPA (2012) estimates that national flowback water volume ranges from 10% to 70% of the injected fluid; Marcellus shale flowback water is in the range of 9% to 15%. Some researchers have attributed the volume loss to fracture fluid being retained in nonconductive portions of the fractures, and in spaces that were previously occupied by salts that were dissolved by the fracture fluid (Gdanski, Weaver et al. 2007; Blauch, Myers et al. 2009).

Even after extended cleanup, post fracture reservoir performance frequently falls below expectations. This outcome has been attributed to fracture, and matrix damage caused by the fracture fluid (Holditch 1979; Sherman and Holditch 1991; Ning, Marcinew et al. 1995; Wang, Holditch et al. 2008). Coexisting with fracture fluid induced damage are other phenomena such as pore volume compaction, gas desorption, and gas slippage; all can potentially increase recovery rates and ultimate recovery (Ertekin, King et al. 1986; Gao, Lee et al. 1994; Chawathe, Ertekin et al. 1996; Clarkson, Nobakht et al. 2012; Yu and Sepehrnoori 2013).

Many researchers have investigated the net effect of several fracture fluid induced damage mechanisms on reservoir performance. However missing from literature are the results of a complete study that not only seeks to capture the mechanisms that most significantly hinder shale gas recovery but also those that enhance this recovery, and net effect of these combined mechanism. The objective of this work is to perform a comprehensive numerical study that will assess the net effect of the mechanisms that hinder fluid clean-up and gas recovery, and the phenomena that enhance this recovery.

Related Literature

The impact of fracture fluids on reservoir performance was recognized as early as the 1950's. Though most agree that these fluids have the potential to damage the formation, the mechanisms that cause this damage, and the relative impact of each on reservoir performance is still being debated. Damage caused by fracture fluid may be classified as damage inside the fracture and damage inside the matrix (Wang, Holditch et al. 2010). Matrix damage is further subdivided into absolute, and relative permeability damage (Ning, Marcinew et al. 1995).

Fracture damage includes, but is not limited to, proppant crushing, proppant embedment, proppant plugging, and proppant diagenesis. Absolute permeability damage in the matrix may result from clay particle swelling or particle migration, polymer invasion, and scale or paraffin precipitation. Relative permeability damage usually accompanies absolute permeability damage, and is the direct result of fluid saturation and rock wettability changes. The following subsections provide background to several important damage mechanisms that will be addressed in this manuscript.

Fracture Fluid Damage. The intent of hydraulic fracturing is to improve well productivity. In 1961, Prats established a relationship between productivity improvement and the fracture conductivity $(k_f w_f)$. This work and later works by Cinco et al showed that the productivity improvement factor is directly proportional to the conductivity ratio (C_r), which in turn is directly proportional to the fracture conductivity $(k_f w_f)$ (Prats 1961; Cinco L, Samaniego V et al. 1978; Cinco-Ley and Samaniego-V 1981). Consequently any mechanism that adversely impacts fracture permeability (k_f), fracture width (w_f), matrix permeability (k) or the fracture length (L_f) will limit improvements in the reservoir productivity.

$$C_r = \left(k_f w_f / \pi k L_f\right) \qquad \text{(1)}$$

In 1979 Holditch used a 2-phase, 2-dimensional model to investigate the effect of fracturing fluid induced permeability damage and capillary pressure changes on reservoir performance. Gdanski used a numerical simulator to study the impact of fracture-face-matrix damage and fracture-face-skin evolution during cleanup, and Wang et al investigated the effect that gel damage, proppant crushing and polymer filter cake formation has on the cleanup process. (Gdanski, Weaver et al. 2005; Wang, Holditch et al. 2008; Gdanski, Fulton et al. 2009; Wang, Holditch et al. 2010). More recently, Osholake, Wang et al, and Abah and Wang used 2-dimensional, 2-phase models to study fracture fluid cleanup and reservoir performance in gas shales (Osholake, Wang et al. 2011; Abah and Wang 2013).

Multiphase Flow Effects. Holditch (1979) stated that invading fracture fluid could damage the reservoir rock permeability and increase capillary pressure in the damage zone. The water pressure in the damage zone will then acts as a water pressure sink that draws water towards this zone. He further stated that if the pressure drawdown in the fracture is not large enough to overcome capillary end effects, or the water mobility (M_w) is so low that the fracture water remains immobile next to the fracture face, the invaded water acts as a blockade that severely curtails gas production.

Fractures are the freeways that transport reservoir fluid to the wellbore. Any mechanism that retards flow along these pathways creates congestion, analogous to "traffic jam", which slows recovery. Besides creating a blockade in the matrix, as pointed out by Holditch (1979), multiphase flow increases pressure losses in the fractures by at least one order of magnitude, especially for gas and liquid phase flow (Penny and Jin 1995). The reduced pressure gradients in the fractures lessen gas recovery rates, and slows fracture fluid cleanup. This increase in pressure loss has been attributed to saturation and relative permeability changes, and the interaction between gas and water molecules as they flow through the fractures. Increasing the water saturation for example reduces the flow area available to gas, and also reduces relative permeability to gas (k_{rg}), which reduces gas mobility (M_g).

$$M_g = \left(k_{rg} k / \mu_g\right) \qquad \text{(2)}$$

Additionally, when two phases such as gas and water flow through fractures, they travel at drastically different velocities because of mobility differences. Consequently they obstruct each other flow, creating an inefficient flow regime that slows gas recovery.

Proppant Crushing. After fracturing, while the well is shut-in, much of the remaining fracture fluid leaks off into the formation reducing the fracture fluid pressure, and thus causes the fractures to close on the proppant. Some of the proppant are deformed, others are crushed, and some are embedded in the walls of the fracture. These effects decrease the fracture conductivity $(k_f w_f)$ by reducing the fracture width (w_f) and the proppant pack permeability (k_f). Proppant damage is further exacerbated during production; continually increasing effective stress in the reservoir caused by fluid extraction, and oscillations in the bottomhole pressure due to well operations, further crushes or deforms the proppant. Proppant pack failure, in the form of proppant crushing, have been studied greatly, and its impact on well performance, typically manifested as reduced well productivity, has been reported on extensively (Cooke 1973; Palisch, Duenckel et al. 2007; Tao, Ehlig-Economides et al. 2009; Osholake, Wang et al. 2011; Han, Wang et al. 2014).

Proppant Diagenesis. Cikes (2000) reported that in high temperature wells, fracture conductivity continued to decrease beyond closure even when high strength proppant was used. He suggested that there must be other mechanisms or factors

that continually drives the reduction in proppant pack permeability besides effective stress. Weaver (2005; 2007) suggested that diagenesis-type reactions between the proppant and fractured rock surfaces create crystalline and amorphous minerals that fill the pore spaces in the proppant pack. The permeability of a proppant pack, and the conductivity of a fracture are strongly dependent on the porosity of the proppant pack. Consequently any reaction or mechanism that reduces the porosity of the proppant pack will significantly reduce fracture conductivity.

Weaver, Nguyen et al (2005) showed that diagenesis-type reactions occur in the reservoir (during cleanup) where temperatures and stress gradients are high. During cleanup and subsequent production, increasing effective stress crushes the proppant and formation material; the freshly exposed faces of these materials in the presence of high-ionic strength fracturing fluids undergo rapid diagenesis-type reactions. These reactions include the dissolution of some proppant minerals, which causes proppant compaction and embedment, and the formation of crystalline overgrowth, which fill pores, and progressively damage proppant pack permeability.

Rock Compaction. Karl Terzaghi theory of effective stress states that if the pores in a soil mass are interconnected and filled with fluid, the effective stress (σ_e) at any point in that system is the difference between the insitu stress (σ_{min}) and the formation pore pressure (p_p). Accordingly any measurable change in the soil mass, such as compaction or distortion, is a direct result of a change in effective stress.

$$\sigma_e = \sigma_{min} - p_p \quad \text{..... (3)}$$

When a reservoir is placed on production, the fluids in the pore volume are depleted; this causes a reduction in the pore pressure (P_p) and a concomitant increase in the formation effective stress (σ_e). As production progresses the effective stress continues to increase and eventually triggers micron scale deformations such as grain contact spreading, cement breakage, grain rotation and sliding, and crystal plastic deformation (Schutjens, Hanssen et al. 2001). These changes are often manifested as porosity reduction in rocks due to compaction. Rock compaction is an important driving force for hydrocarbon production because it pushes fluids towards the wellbore thus improving recovery (compaction drive). The Achilles heel of compaction drive recovery is that it leads to land subsidence, and it is also accompanied by a reduction in porosity, which limits reservoir rock permeability.

Gas Desorption. Shale formations, such as the Devonian Marcellus shale deposits, store a large portion of their gas in place as adsorbed gas in the low permeability matrix (Gao, Lee et al. 1994; Fathi and Akkutlu 2012). The gas is gradually released into the pore spaces and fractures as the reservoir is depleted.

$$V_E = \frac{V_L p_g}{p_L + p_g} \quad \text{..... (4)}$$

Gas adsorption/desorption is a function of reservoir pressure, and is normally incorporated in reservoir simulators using the Langmuir equation. The total volume of gas adsorbed per unit volume of reservoir (V_E) is a function of the Langmuir volume (V_L), the Langmuir pressure (p_L), and the reservoir gas pressure (p_g). While the impact of shale gas desorption on short-term recovery is slight, its impact on long-term ultimate gas recovery is significant, and thus it must be accounted for in any realistic shale gas model.

Gas Slippage. The permeability of a core is typically determined using dry air. Prior to Klinkenberg experiments in 1941, based on the premise that the permeability constant of a porous medium is a function of the medium and independent of the fluid, the experimentally determined permeabilities were though to apply to the flow of either gas or oil in the reservoir. However, Klinkenberg showed that when a gas is used as the testing fluid, the calculated permeability is greater than the true absolute permeability (k) of the rock. He attributed this observation to gas slippage along the wall of the porous medium. He also concluded that the apparent gas permeability (k_a) was not a constant but a function of the gas slippage factor (b), and the reciprocal mean flowing pressure ($\bar{p}$).

$$k_a = k\left(1 + \frac{b}{\bar{p}}\right) \quad \text{..... (5)}$$

Klinkenberg results also indicated that the slippage factor(b) varies with pressure. However the slippage factor is treated as a constant in many applications today.

As a gas reservoir is depleted, the reservoir pressure falls concurrently, and therefore the gas slippage effect will vary throughout the life of the reservoir. To account for the apparent increase in permeable of sample during gas phase flow, Ertekin, King et al (1986) proposed that gas flow in low permeability formations was due to both pressure and concentration gradients. They further postulated that these forces act in parallel and therefore their superficial velocity vectors are additive (v^T).

$$\nu_\alpha^{\mathrm{T}} = \nu_\alpha^{\mathrm{D}} + \nu_\alpha^{\mathrm{s}} \quad \text{..... (6)}$$

$$-\nabla(\rho_\alpha \nu_\alpha^T) + Q^* = \frac{\partial}{\partial t}(\emptyset \rho_\alpha S_\alpha) \quad \text{..... (7)}$$

$$b_a = \frac{S_g p_g c_g \mu_g D_c}{\beta k_{rg} k_\infty} \quad \text{..... (8)}$$

Equations 6 and 7 *(continuity equation)* illustrate their hypothesis. Equation 8 outlines their apparent gas-slippage factor (b_a), which is not constant, as previously shown by

Klinkenberg (1941), but a function of pressure, composition, temperature and saturation (Ertekin, King et al. 1986).

Reservoir Model

There are two natural fracture networks that are reinitiated during fracturing in Marcellus shale: *J1 fractures*, which are approximately 1 ft. apart, and the *J2 fractures* which are 2 ft. apart. This type of reservoir structure is ideally suited for the dual-porosity concept proposed by Warren and Root (1963).

To achieve the objective of this paper, a 2-phase, 3-dimensional, dual-porosity reservoir simulator was written and validated; the details of this model are presented in Part I of this work. The model output is based on the simultaneous solution of the gas and water continuity equations **(Eq. 9 to Eq. 14)** for pressure and saturation using upstream transmissibilities; the equations are presented in 1 Dimension for clarity. The To reduce stability issues the simulator was written as a fully implicit model; gas pressure and water saturation in the fractures and matrix blocks, and gas and water flow rates are all solved simultaneously and implicitly at each time step.

Matrix Gas Equation

$$(\sigma V_b)\left\{(\beta_c)(k_{ma})\left(\frac{k_{rg}}{\mu_g}\right)\left(\frac{p_g}{z}\right)\left[(p_g)_{frac}-(p_g)_{matrix}\right]+\frac{D_c}{\alpha_c}\left[\left(\frac{S_g p_g}{z}\right)_{frac}-\left(\frac{S_g p_g}{z}\right)_{matrix}\right]\right\} = \frac{V_b}{\alpha_c}\frac{\partial}{\partial t}\left[\left(\frac{\phi S_g p_g}{z}\right)+\left(V_E\frac{T p_{sc}}{T_{sc}}\right)\right]_{matrix} \quad \text{..... (9)}$$

Matrix Water Equation

$$T_{wMa-F}\left[(p_w-\gamma_w Z)_{frac}-(p_w-\gamma_w Z)_{matrix}\right] = \frac{V_b}{\alpha_c}\frac{\partial}{\partial t}\left(\frac{\phi S_w}{B_w}\right)_{matrix} \quad \text{..... (10)}$$

Fracture Gas Equation

$$\frac{\partial}{\partial x}\left[\beta_c A_x k_x k_{rg}\frac{p_g}{\mu_g z}\left(\frac{\partial p_g}{\partial x}\right)+\frac{D_{cx}A_x}{\alpha_c}\frac{\partial}{\partial x}\left(\frac{S_g p_g}{z}\right)\right]\Delta x + \frac{p_{sc}T}{\alpha_c T_{sc}}q_{gsc}-T_{gMa-F}\,\Delta_{gF-Ma}(p_g) - \frac{(V_b\sigma)D_c}{\alpha_c}\Delta_{g\_F-Ma}\left(\frac{S_g p_g}{z}\right) = \frac{V_b}{\alpha_c}\frac{\partial}{\partial t}\left(\frac{\phi S_g p_g}{z}\right)_{fracture} \quad \text{..... (11)}$$

Where

$$T_{gMa-F}=\beta_c(V_b\sigma)k_{Ma}\left(\frac{p_g}{z\,\mu_g}\right)(k_{rg})_{upstream} \quad \text{..... (12)}$$

Fracture Water Equation

$$\frac{\partial}{\partial x}\left[\beta_c k_x A_x\frac{k_{rw}}{\mu_w B_w}\left(\frac{\partial p_w}{\partial x}-\gamma_w\frac{\partial Z}{\partial x}\right)\right]\Delta x + q_{wsc} - T_{wMa-F}\Delta_{w\_F-Ma}(p_w-\gamma_w Z) = \frac{V_b}{\alpha_c}\frac{\partial}{\partial t}\left(\frac{\phi S_w}{B_w}\right)_{fracture} \quad \text{..... (13)}$$

Where

$$T_{wMa-F}=\beta_c V_b\sigma\left(\frac{k_{Ma}}{\mu_w B_w}\right)(k_{rw})_{upstream} \quad \text{..... (14)}$$

Model Validation. Model development, along with validation results, is presented in other works by the authors (Part I). However, for completeness, validation results are summarized here. The developed numerical simulator was validated through 2 successive steps: (1) internal validation, and (2) external validation. Since the fluid transport equations **(Eq. 9** to **Eq. 14)** are based on the principle of mass conservation, a mass balance check of the solution attained at each time step shows whether mass is conserved. If so, the solution is deemed correct in this regard. Mass balance is essentially the ratio of net change to net throughput; this value should be equal to 1, within at least 4 decimal places. Internal validation involves both incremental (at the end of each time step), and cumulative (over time (t) from t = 0 to t = current time) mass balance checks. The equations used to complete these checks for water are presented as **Eq. 15** and **Eq. 16**; similar equations were implemented to complete the mass balance checks for the gaseous phase.

Incremental Mass Balance Check (IMBC) for water

$$\text{IMBC}=\left[\frac{\sum_{k=1}^{N_z}\sum_{j=1}^{N_y}\sum_{i=1}^{N_x}\left[\left(\frac{V_b\phi S_w}{\alpha_c B_w}\right)_{Ma\,\&\,F}^{n+1}-\left(\frac{V_b\phi S_w}{\alpha_c B_w}\right)_{Ma\,\&\,F}^{n}\right]}{\sum_{k=1}^{N_z}\sum_{j=1}^{N_y}\sum_{i=1}^{N_x}(q_{wsc})_{i,j,k}^{n+1}\,\Delta t}\right] \quad \text{..... (15)}$$

Cumulative Mass Balance Check (CMBC) for water

$$\text{CMBC}=\left[\frac{\sum_{k=1}^{N_z}\sum_{j=1}^{N_y}\sum_{i=1}^{N_x}\left[\left(\frac{V_b\phi S_w}{\alpha_c B_w}\right)_{Ma\,\&\,F}^{n+1}-\left(\frac{V_b\phi S_w}{\alpha_c B_w}\right)_{Ma\,\&\,F}^{t=0}\right]}{\sum_{l=1}^{m}\sum_{k=1}^{N_z}\sum_{j=1}^{N_y}\sum_{i=1}^{N_x}(q_{wsc})_{i,j,k}^{n+1}\,\Delta t_l^m}\right] \quad \text{..... (16)}$$

After acceptable mass balance results were achieved, external validation was accomplished by comparing the model outputs to those from an external source. Chawathe (1995), and Chawathe, Ertekin et al (1996) in their work on multimechanistic flow in fractured reservoirs presented gas and water flow rates, and well block pressures predicted by

their dual-porosity model. Chawathe and Ertekin (1996) model inputs, along with their simulated outputs, were used to externally validate our numerical simulator. Input parameters for the dual porosity system are presented in **Table 1**.

Simulation Parameters	Parameter Value
Fracture Variables	
System size	5 x 5 x 1
Block size (x)	500 ft.
Block size (y)	500 ft.
Block size (z)	100 ft.
Initial Water Saturation (Swi)	0.3
Fracture Permeability	1000 mD
Fracture Porosity	1%
Initial Reservoir Pressure (pi)	4000 psi
Sandface pressure (psf)	3500 psi
Well Radius (rw)	0.25 ft.
Well Skin factor (S)	0
Matrix Variables	
Block size (x)	500 ft.
Block size (y)	500 ft.
Block size (z)	100 ft.
Initial Water Saturation (Swi)	0.3
Matrix Permeabiilty	0.01 mD
Matrix Porosity	0.19

Table 1: Dual Porosity validation input parameters

The convergence criterion set for the numerical solutions, based on a fully implicit approach, was 0.0001 psi. The incremental and cumulative mass balance checks, for the external validation simulation, are presented in **Fig. 1** and **Fig. 2**. In both cases, the mass balance falls within the range 1.0000001 and 0.9999999; these results suggest that the model is working excellently from the standpoint of mass conservation. Additionally, the model residuals for all calculated pressures and saturations fall below 10^{-8}, which further supports the correctness of the mathematical equations, and accuracy of the convergence criteria incorporated in the model.

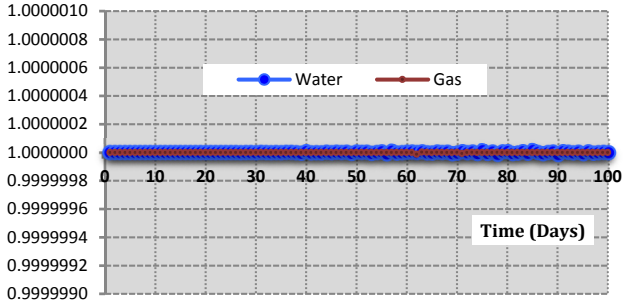

Fig. 1: Incremental Material Balance Check (IMBC)

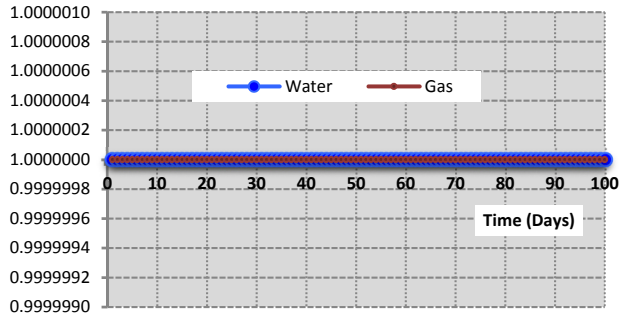

Fig. 2: Cumulative Material Balance Check (CMBC)

To complete the external model validation, the output pressures and saturations published by Chawathe and Ertekin were extracted from their published plots (digits not published), represented in figures 3 to 6, and titled validation data (blue squares). Interested readers are referred to "Development and testing of a dual-porosity, dual-permeability simulator to study multimechanistic flow through tight, fractured reservoirs" by Chawathe and Ertekin (1995) for the original data set and published plots. Comparison of the gas and water flow rates, presented in **Fig. 3** and **Fig. 4**, show good agreement between the validation and simulated flow rates. The simulated reservoir volume is 6.25 x 10^8 cu.ft and the initial water in place is 3.5 x10^7 cu.ft. The average difference between our model and Chawathe's model is less than 1 bbl water (5.6 cu.ft). This is less than 0.000003% of the water in place; the numbers are better for the gas phase and is evident from Fig. 3.

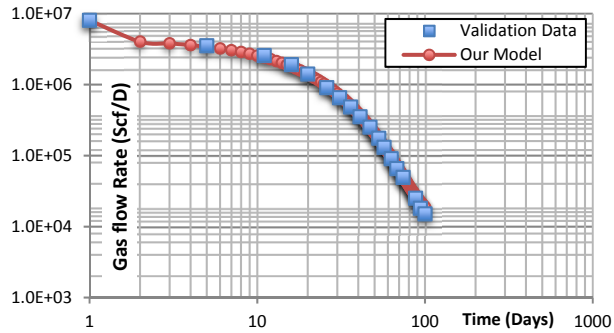

Fig. 3: Dual Porosity Validation – Daily gas flow rate

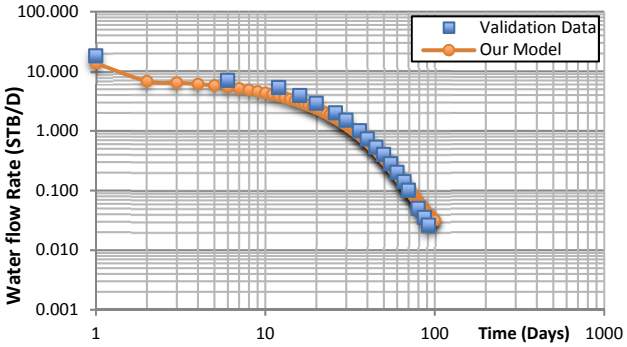

Fig. 4: Dual Porosity Validation – Daily water flow rate

Since the simulator was developed using the dual-porosity concept (reservoir separated into 2 domains: matrix and fractures), the simulated matrix and fracture domain pressures must also to be compared to those from the external source. The well block simulated matrix and fracture domain pressures were compared to the validation data and presented in **Fig. 5** and **Fig. 6**. Again, the simulated outputs showed a good match to the validation dataset. Minor variations in the pressure profile is attributed to different solution techniques; our model used a fully implicit approach to determining pressure and saturation versus the implicit pressure explicit saturation (IMPES) approach used in the validation data set. The largest pressure difference between the two models in matrix domain is seen at day 15. Our model predicted 3717psi, Chawathe model predicted 3670psi. The percentage difference seen on this day, relative to Chawathe predicted pressure, is 1.28%. In the fracture domain, the largest pressure difference between the two models was 1.2 psi or 0.034% relative to the fracture domain pressure predicted by Chawathe's model.

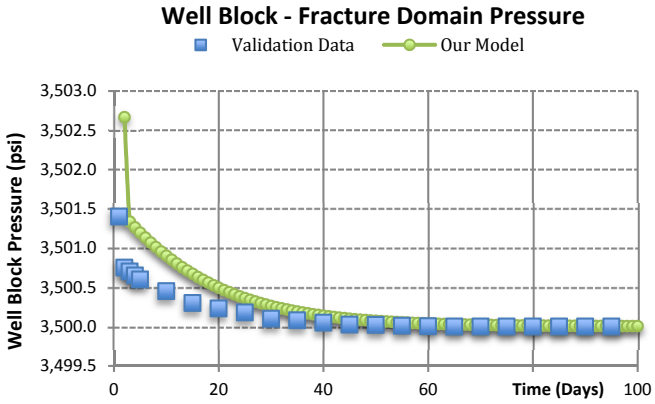

Fig. 5: Dual Porosity Validation – Well Block Fracture Domain Pressure

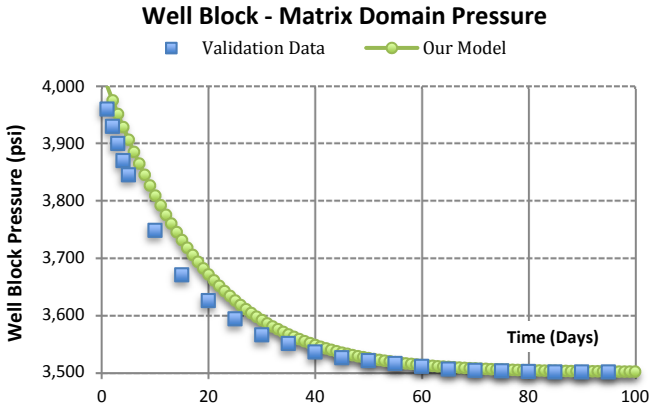

Fig. 6: Dual Porosity Validation – Well Block Matrix Domain Pressure

The fluid transport module presented above is part of larger fully coupled numerical simulator that has two other modules, which simulates dissolve species concentration in flowback water, and halite dissolution in the formation respectively. Compared to other approaches, the fully implicit approach generates more accurate solutions (pressure, saturation, flow rate) to the continuity equations presented above. Since the outputs (pressure, saturation, and flow rates) from the fluid transport model are direct inputs into the ion transport module, a fully implicit approach was selected to minimize error amplification in the ion transport, and flowback water dissolve species results.

Numerical Modeling. There are currently no empirical models that can predict the change in proppant pack permeability caused by proppant diagenesis. However, experimental work done by Lee, Elsworth et al (2009) and later incorporated by Osholake, Wang et al (2011) provides guidance on the potential impact diagenesis can have proppant pack permeability. These published experimental data are incorporated into the model to capture the effects of proppant diagenesis (Refer to **Fig. 30**). Unlike proppant diagenesis, there are several empirical formulations that have been developed to predict the effect of proppant crushing, and reservoir rock compaction on fracture and matrix properties as a function of effective stress (Schutjens, Hanssen et al. 2001; Reyes and Osisanya 2002; Han, Wang et al. 2014). However, to avoid incorporating the assumptions inherent in these models in our simulation, we opted to include experimental data that captures proppant pack permeability change caused by proppant crushing (Refer to **Fig. 27**).

The change in pore volume due to changing effective stress is captured through the pore volume compressibility coefficient (c_p). C_p can also be expressed in terms of porosity (ϕ), as illustrated in equations 17 and 18; equation 18 was used to capture porosity change in the reservoir model caused by changing effective stress.

$$c_f = c_p = \frac{1}{V_p}\left(\frac{\partial V_p}{\partial p}\right)_T = \frac{1}{\phi}\frac{\partial \phi}{\partial p} \quad \text{..... (17)}$$

$$\phi = \phi_0\left(1 + c_f(p - p_0)\right) \quad \text{..... (18)}$$

Based on work by Ertekin, King et al (1986), King (1985) showed that the superficial velocity for gas (v_t), due to both Darcian and Fickian flow in a rectangular coordinate system, is given by equation 19.

$$v_t = -\frac{D_x z}{P_g}\frac{\partial}{\partial x}\left(\frac{P_g S_g}{z}\right) - \frac{\omega^* k_x k_{rg}}{\mu_g}\frac{\partial P_g}{\partial x} \quad \text{..... (19)}$$

Using this derivation along with the continuity equation, Langmuir equation, and Warren and Root Dual Porosity concept, the flow equations for the gas and water phases in both the matrix and the fractures (**Eq. 9 to Eq. 14**) were

developed. Details on the development of these equations are presented in Part I of this work.

Field Model Simulation. The simulated reservoir was based on a traditional shale gas pad layout; six (6) laterals, each approximately one (1) mile long, feed gas to a single well pad (**Fig. 7**). Our model focused on capturing the stimulated area for a single lateral (Fig. 7). Using symmetry, one half of the area depleted was modeled (**Fig. 8**). The numerical grid system is nonuniform and is locally refined around the hydraulic fractures to adequately capture the rapid change in pressure and saturation that was anticipated in the vicinity of the fractures. The grid dimensions varies in a logarithmic fashion away from the completion towards the extremes of the simulated reservoir where pressure and saturation changes are more gradual or insignificant. Interested readers are referred to the "Analysis of Fracture Fluid Cleanup and Long-Term Recovery in Shale Gas Reservoir" and "Development of a Halite Dissolution Numerical Model for Hydraulically Fractured Shale Formations (Part I)", both by the authors, for further details. These manuscripts give a detailed description on model development from fundamentals to the continuity equation, discretization and reservoir gridding, equation linearization, solution techniques, and model convergence criteria.

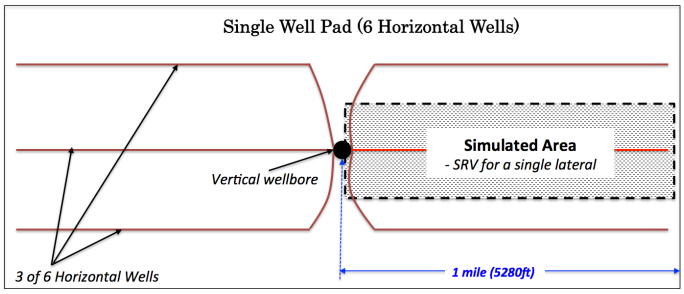

Fig. 7: Stimulated area for a single well pad (5280ft x 2640ft)

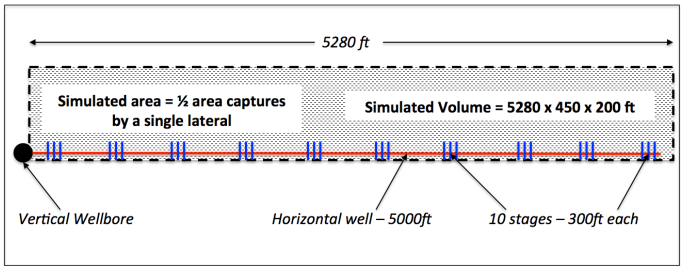

Fig. 8: Illustration of the simulated reservoir layout

In the model, we assumed a preexisting fracture network that was created from a ten (10) stage hydraulic fracturing process; each stage is 300ft in length and has three (3) completion clusters that are evenly spaced (Fig. 8). The spacing of the natural fractures in the SRV were assumed to follow Marcellus J1 and J2 fractures, which are 1ft and 2ft apart respectively. To allow for a more realistic saturation distribution in the reservoir, 220,000 gallons of fracture fluid was injected into each stage sequentially, starting with the stage furthest from the wellbore. It was assumed that the injection process had a negligible impact on reservoir temperature, for a relatively short time, on a small reservoir volume, and therefore the process is isothermal. This being the case, changes in reservoir rock and reservoir fluid volume, brought on by temperature changes is negligible and can be omitted from the simulation. Since Marcellus shale reservoir temperatures range from about 100 °F to 150 °F (Halliburton, 2009), the simulated reservoir was assumed to have a temperature of 130 °F. It was also assumed that the reservoir is homogeneous and isotropic with respect to temperature. Other Relevant simulation parameters are presented in **Table 2**.

Simulation Parameters	Parameter Value
Formation Depth (ft)	5000
Reservoir Temperature (°F)	130
Simulated area (ft)	5280 x 450
Reservoir thickness (ft)	200
Natural fracture spacing (ft)	2 x 1
Initial reservoir pressure (psi)	3500
Initial gas saturation (%)	90
Matrix permeability (mD)	0.0001
Hydraulic fracture conductivity (md-ft)	420
Matrix porosity (%)	3
No. of stages	10
Langmuir pressure (psi)	673
Langmuir volume (scf/ton)	115
Completion clusters per stage	3
Fracture fluid per stage (gallons)	220,000
Proppant type	100 mesh sand
Sandface pressure (psi)	1000
Skin factor	0
Well radius (ft)	0.25

Table 2: Model Simulation parameters

Results and Discussion

Multiphase Flow Effects. For the purpose of comparison, the first simulation is single-phase gas. For this simulation only, simply for the purpose of comparison, no fluid was injected. Doing otherwise would have changed the reservoir saturation profile and the ensuing flow regime. The intent here is to demonstrate the impact that saturation changes, caused by hydraulic fracturing, have on gas recovery rate and cumulative gas recovered. For this single phase simulation, the reservoir was flowed for 27 years at a specified sandface pressure of 1000 psi. The gas recovery rates and cumulative gas recovered were compared to those predicted from our multiphase flow simulation; the results are presented in **Fig. 15** and **Fig. 20**.

For the multiphase flow case, as outlined above, 220,000 gallons of water was injected into each stage sequentially, starting with the stage furthest from the wellbore. The capillary pressure and relative permeability plots used in the multiphase models are presented in **Fig. 9** and **Fig. 10.** The shale matrix pressures and saturations recorded during the injection phase are presented in **Fig. 11** and **Fig. 12**. For clarity, these figures show only 1 stage, with 3 completion clusters. It should be noted that for this multiphase flow scenario, the effects of other physical and chemical phenomena, such as proppant crushing, proppant diagenesis, rock compaction etc. were excluded from this model. Such phenomena were studied separately, and the results are presented later in this manuscript. The intent of this multiphase section is to demonstrate the impact that saturation changes, caused by hydraulic fracture, have on shale gas recovery rate and the ultimate gas recovered.

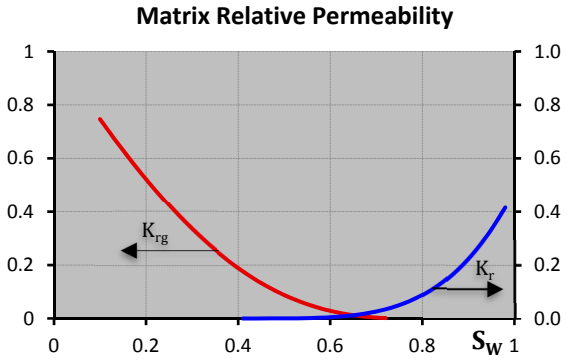

Figure 9: Matrix relative permeability profiles

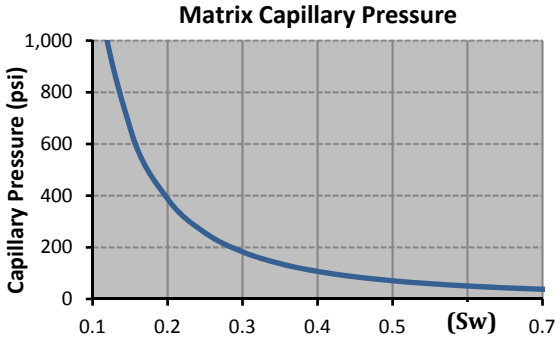

Figure 10: Matrix capillary pressure profile

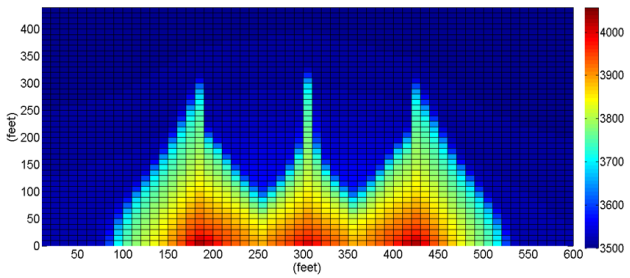

Figure 11: Reservoir gas pressure (psi) during injection (NTS)

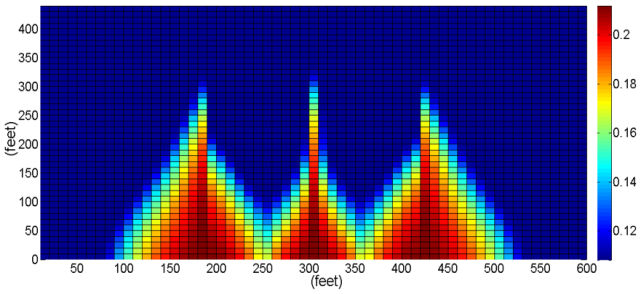

Figure 12: Reservoir water saturation during injection (NTS)

Fig. 13 and **Fig. 14** compare the recovery rate and cumulative recovery respectively, for the gas and liquid phases. Fig. 13 shows, as the recovery rate for the liquid phase plummets, the gas recovery rate promptly increases. This observation is related to the relative permeability (refer to Fig. 9) between the two (2) phases. A reduction in water saturation results in a higher relative permeability to gas (k_{rg}) and therefore higher gas recovery rates. As **Fig. A1** in the appendix shows, the water saturation in the fractures, which are the primary conduits for fluid recovery in a shale formation, quickly falls off, giving rise to a higher gas phase saturation and therefore higher k_{rg} values.

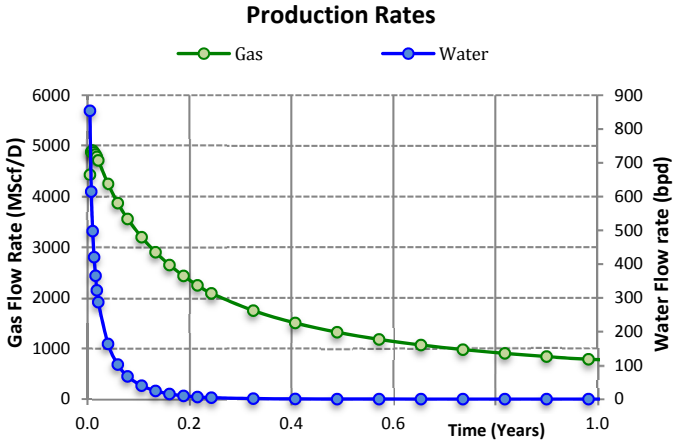

Fig. 13: Gas and water production rate

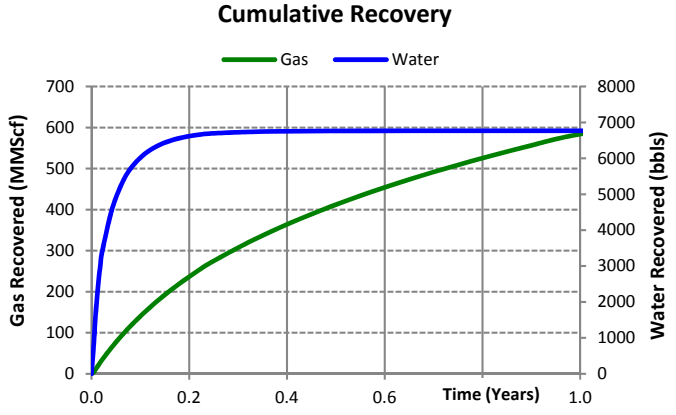

Fig. 14: Gas and water cumulative recovery

In regards to cumulative recovery, Fig. 14 shows that most of the injected fluid, approximately 6,500 bbls, is recovered within the first 60 days of production. Our results, presented in the Injected Fluid Recovery section of this manuscript, suggest that the timeframe, and volume of injected fluid recovered is a strong function of the high capillary pressure forces existing in the rock matrix (refer to fig. 10). These capillary pressure forces drive imbibition, and trap the injected fluid in the shale rock matrix (refer to **Fig. 39**) thereby limiting cumulative recovery. **Fig. A2** and **Fig. A3,** shown in the appendix, support this hypothesis. These figures show a substantial increase in both the fluid recovery rate and the percentage of injected fluid recovered, when the simulation assumes zero capillary pressure in the rock matrix. If no capillary pressure forces existed in the rock matrix, Fig. A3 shows that approximately 53% of the injected fluid will be recovered in the first year of production compared to only 13% if capillary pressure forces were captured in the simulation. This observation clearly illustrates the role capillary pressure forces play in fracture fluid cleanup.

As it relates to the comparison between single-phase and multiphase flow, there are two point of interest in **Fig.15**: (1) the high initial gas flow rate for the single-phase model, and (2) the increase followed by gradual decrease in the gas flow rate for the multiphase model. Since we had to assume a preexisting active fracture network, the highly permeable fractures are filled with gas for the single-phase model. The gas in these fractures is not limited by the low matrix permeability (0.0001mD) but is driven by the high fracture conductivity (420 md-ft). Accordingly, any gas initially located in the fractures is produced rapidly within the first few days of production. Production rate slows as gas begins to flow from the matrix to the fractures; flow rate at this point is now predominantly governed by the low matrix permeability and not the high fracture conductivity.

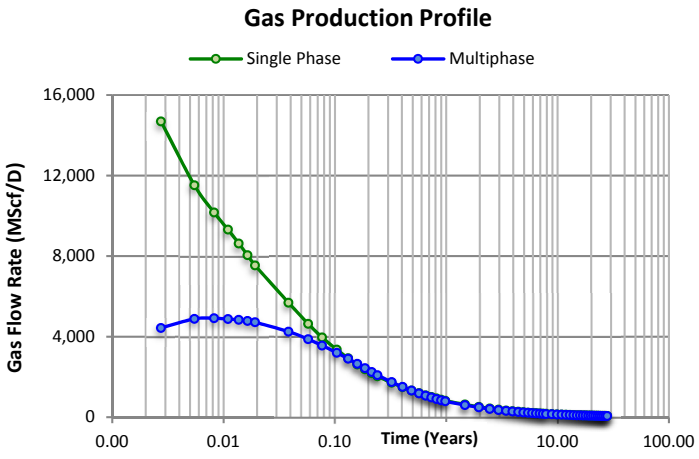

Fig. 15: Gas production rate for single and multiphase flow

In the multiphase flow scenario, prior to flow back, the fractures are almost 100% filled with water instead of gas because the system is flooded (water injected) before flow back commences. As stated previously, this is done to allow for a more realistic water saturation distribution in the reservoir prior to flow back. Accordingly, high water saturation in the fractures essentially means low gas volumes, low gas saturation, and low permeability to gas (refer to Fig. 9) in the said fractures. These are the primary reasons for the disparity seen between the initial gas flowrate for the single phase versus multiphase flow scenarios.

Fig. A4, presented in the appendix, supports the hypothesis in the preceding paragraph. This figure illustrates the change in the gas volume in the fractures of the SRV during the first production year. Fig. A4 shows that the gas in place in the fractures for the single-phase simulation (~16 MMscf) is almost double that found in the same fractures at the start of production (following injection) for the 2-phase simulation. This substantial difference in the volume of gas found in the fractures prior to production, explains the differences in initial gas recovery rate seen in Fig. 15 for the single-phase versus multiphase flow simulation. Fig. A4 also shows that volume differences quickly dissipate after 0.1 years, approximately the same time that recovery rate differences disappear in Fig. 15.

The prompt increase in gas flow rate seen in the multiphase model, during the first few days of production, was caused by quick transitioning from a flow regime dominated by water to one dominated by gas, as illustrated in **Fig. 16**. Fracture fluid injection saturated many of the fractures and rock matrix surrounding the completion clusters. High water saturation in the fractures, during initial production, caused low permeabilities relative to gas (k_{rg}) that restricted gas flow rates (refer to **Fig. 17**). However, this water was either produced, or quickly imbibed into the matrix blocks due to high capillary pressures (refer to Fig. 39). These processes, both production and imbibition, caused a quick change in the saturation profile in the fractures, from almost 100% water to nearly 100% gas (refer to Fig. 16). Similar to the single-phase simulation, gas in the fractures is produced rapidly then flow rate slows as gas begins to flow from the low permeability matrix to the fractures.

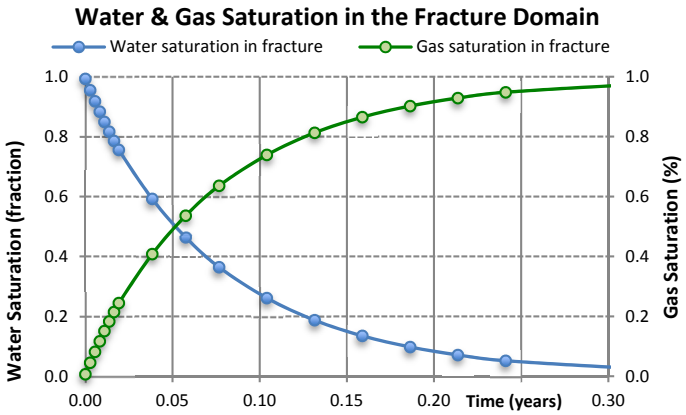

Fig. 16: Gas and water saturation in the fracture domain

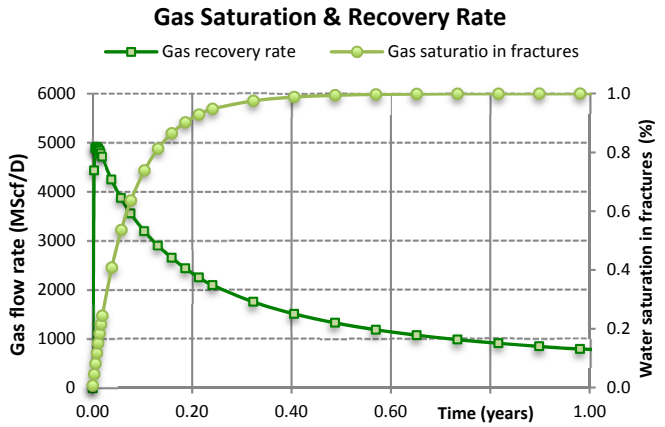

Fig. 17: Gas recovery rate vs. gas saturation in the fracture domain

Although gas flow rates for the single and multiphase models are initially significantly different (Fig. 15), this difference quickly diminishes after one month of production. However, minor flow rate differences between the two models, caused by permanent matrix saturation changes (refer to Fig. 39), cause the multiphase model to produce 143 MMScf (7%) less gas than the single-phase model after 27 years (refer to **Fig. 20**). At an average gas price of $3.5/Mscf, this difference may be considered insignificant over such an extended period. However if we were to consider that this difference represents only ½ of the cumulative production of a single lateral, and each well pad may have 6 laterals, and each field may have several well pads, the economics of this situation quickly reverses. **Fig. 18** and **Fig 19** (NTS) show that even as the well is produced and reservoir pressure falls, some of the water that imbibed into the shale matrix during injection remains trapped. The affected matrix blocks do not return to their original 10% insitu water saturation. It has also been observed that water continues to imbibe in many of the numerical matrix blocks, even during flow back. The increasing water saturation (S_w) further reduces k_{rg} (refer to Fig. 9) and curtail gas recovery from these blocks. These observations are discussed further under the combined mechanism section of this manuscript. These permanent matrix saturation changes, as indicated above, are one of the reasons for the difference in cumulative gas recovered between the single and multiphase models presented in **Fig. 20.**

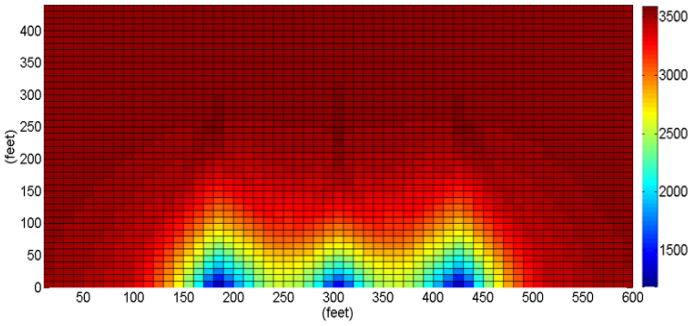

Figure 18: Reservoir gas pressure (psi) during flow back (NTS)
(Multiphase flow scenario)

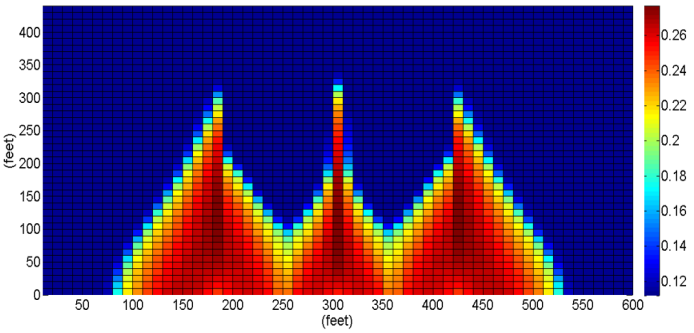

Figure 19: Reservoir water saturation during flow back (NTS)
(Multiphase flow scenario)

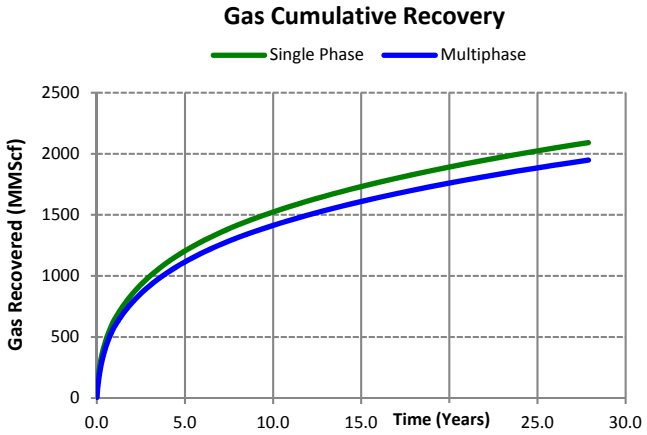

Fig. 20: Gas Cumulative Recovery for single and multiphase flow

Impact of Shut-in Time: Based on our numerical experiments, the results presented in **Fig. 21** shows that the percentage of fracture fluid recovered is inversely proportional to shut-in time. Therefore, the longer the shut-in time, the greater is the percentage of fracture fluid that imbibes from the fractures into the rock matrix. This observation is directly related to the strong capillary pressure forces in the matrix (Fig. 10) that drives imbibition and traps the injected fluid in the reservoir rock (refer Fig. 39). Prior to production, there are no drawdown forces pulling the injected fluid back to wellbore; imbibition is the only force acting on the injected fluid, drawing this fluid into the rock matrix where it becomes trapped. Consequently, as shut-in time increases the volume of injected fluid that is trapped in the matrix increases and percentage of fracture fluid recovered declines (refer to Fig. 21).

The fracture fluid that imbibed into the rock matrix changes the relative permeability dynamics within the formation, and theoretically should cause a reduction in reservoir fluid recovery rates and ultimate recovery. However, in the case of Marcellus shale gas reservoirs, our results suggest that even though fracture fluid leakoff increases with shut-in time, shut-in time does not severely impact gas cumulative recovery in the long-term (Refer to **Fig. 22**). This

result may appear to contradict to our findings in **Single-Phase vs Multiphase phase flow** presented above, but in reality it do not.

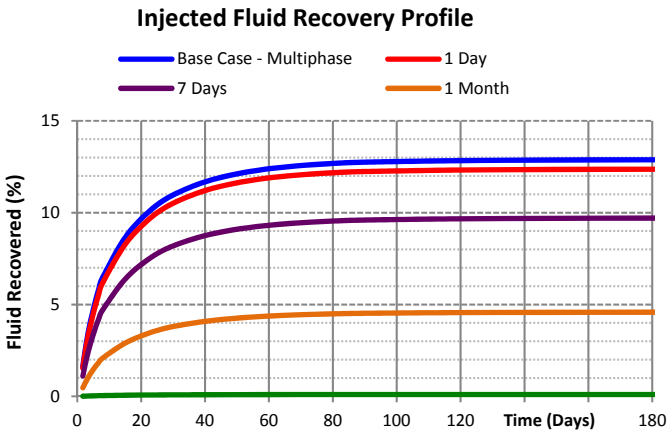

Fig. 21: Injected Fluid recovered as a function of Shut-in time

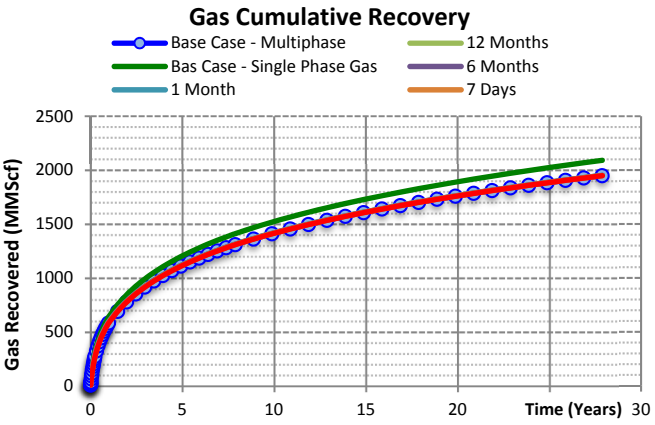

Fig. 22: Cumulative as recovered as a function of Shut-in time

In single-phase gas flow, there are no relative permeability effects to curtail gas recovery. However, the inclusion of a second phase, as is seen in the *multiphase model* above, "shocks" the system by reducing relative permeability to gas (k_{rg}). Further reduction in k_{rg}, and thus smaller gas recovery rates, requires greater and greater increases in water saturation (S_w); this is illustrated in **Fig. 9**. In our analysis of shut-in time, we observed that the difference in matrix water saturation $(S_{w_{ma}})$ seen when the well is flowed back immediately compared to that seen when the well is shut-in for a period prior to production, is not substantially different. This is demonstrated in **Fig. 23,** which illustrates the change in matrix water saturation across time for each of the six (6) simulations. Fig. 23 shows that differences in matrix water saturation across the six models are less than 1% after 60 days. This observation can be attributed to high matrix capillary pressure, which causes water to continually imbibe into the matrix even after production commences. Therefore, since the matrix water saturation among the six models is not substantially different after 60 days, then the difference in matrix k_{rg} among the six models will also not be substantially different after 60 days of production. Consequently, since there is no substantial difference in the relative permeability to gas (k_{rg}) among the six model after 60 days, long-term cumulative gas recovery should not be substantially different as the results in Fig. 22 shows.

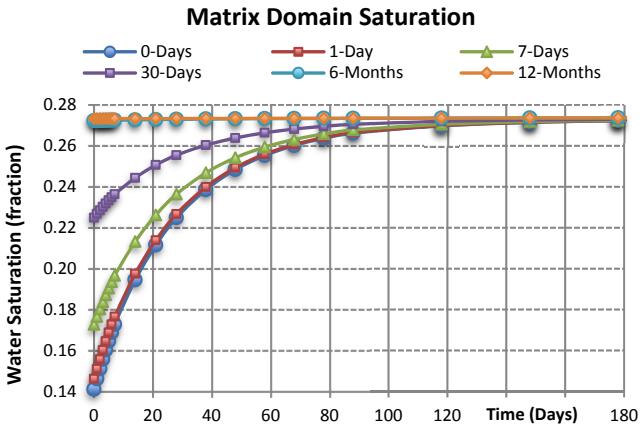

Fig. 23: Matrix domain saturation as a function of Shut-in time

Within the first week of production, **Fig. 24** shows that the longer the shut-in period, the higher is the initial gas flow rate. The longer the well is shut-in, the greater the volume of fracture fluid that leaks off from the fractures to the matrix. Therefore, as shut-in time increases, S_w in the fractures becomes smaller as **Fig. 25** shows. Consequently, as S_w becomes smaller, S_g in the fracture becomes larger and relative permeability to gas (k_{rg}) in the fractures becomes greater. Since initial gas recovery is from the fracture domain, initial recovery rates tend to be higher with increasing shut-in time. However, as initial gas in the fractures is depleted, and gas begins to flow from the matrix to the fractures, gas flow rate falls just below the base model (*0 days shut-in*); refer to Fig. 24. The change in recovery rates explains the similarity seen in cumulative gas recovered among the six models presented in Fig. 22; it is caused by increased water saturation in the matrix (refer to Fig. 23), which is a direct result of the well being shut-in prior to production.

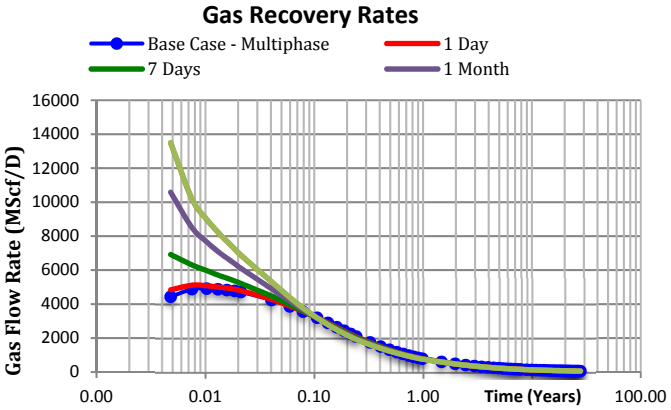

Fig. 24: Gas Recovery Rates as a function of Shut-in Time

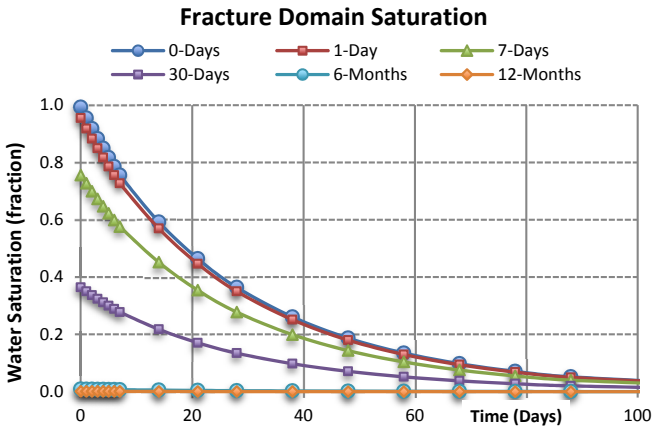

Fig. 25: Fracture domain saturation as a function of Shut-in time

Impact of Gas Desorption: Langmuir desorption parameters (P_L & V_L) vary from one shale deposit to the next, but as **Table 3** shows, these parameters can vary within a single shale deposit such as the Marcellus shale. Each set of parameters, including the average values, were included in our simulator to assess the potential impact of desorption on gas recovery in Marcellus shale. The results of this assessment are presented in **Fig. 26 and Table 4.** Fig. 26 shows the Langmuir volume presented by Wu and Sepehrnoori (2013) is likely to be on the high side of the adsorbed gas present in Marcellus deposits whereas that presented by Boulis, Jayakumar et al (2012) is most probably on the lower end of the spectrum. Godec, Koperna et al (2013) stated that the Langmuir parameters presented was the average of several Marcellus shale samples tested. Unexpectedly, as Fig. 26 shows, the cumulative gas recovery profile generated from Godec, Koperna et al (2013) Langmuir parameters is almost identical to that generated from the average values presented in Table 3.

Langmuir Parameters for Marcellus Shale

No.	Langmuir Pressure P_L (psi)	Langmuir Volume V_L (scf/ton)	Source
1	500	200	Yu and Sepehrnoori (2013)
2	1000	90	Godec, Koperna et al (2013)
3	520	55	Boulis,Jayakumar et al (2012)
4	**673**	**115**	**Average**

Table 3: Langmuir Parameters for Marcellus Shale

Yu and Sepehrnoori (2013), after performing a numerical study that investigated the impact of gas desorption and rock geomechanics on the performance of both Barnett Shale and Marcellus shale reservoirs, found that in both shale deposits, gas desorption can contribute as much as 20% of the 30-year estimated ultimate recovery. Cipolla, London et al (2010) investigated the impact of gas desorption on the production profile and ultimate gas recovery in both the Barnett and Marcellus shale reservoirs at various fracture spacing. They found that at large hydraulic fracture spacing (600 ft. apart) desorbed gas contributed 8.5 % of the total gas recovered after 30 years when the matrix permeability was 0.0001mD and 6.9% when the permeability was 0.00001 mD.

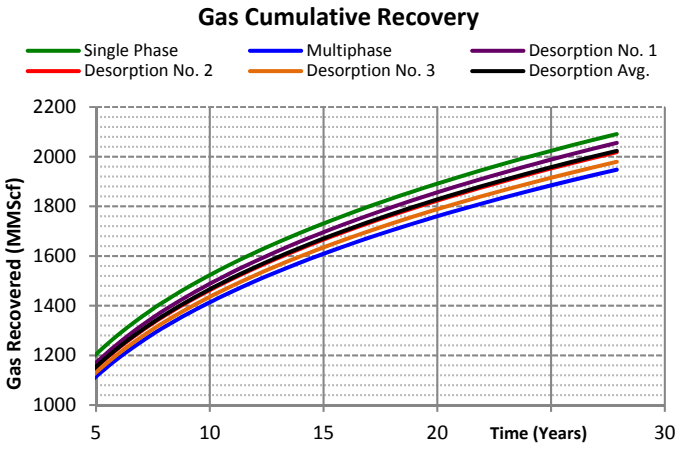

Fig. 26: Impact of Gas Desorption on Cumulative Gas Recovered

Table 4 shows that gas desorption can potentially account for 1.6% to 5.5% increase in cumulative gas recovered in Marcellus shale after 27 years. Base on these results, a single well pad with six laterals can recovery 380MMScf to 1.3Bcf of shale gas after 27 years due to gas desorption alone. However, to be conservative, all future analysis involving gas desorption in this paper will utilize the average Langmuir parameters presented in Table 3.

Gas Recovery Influenced by Desorption

No.	P_L (psi)	V_L (scf/ton)	Gas Recovery (MMScf)	Difference (MMScf)	Difference (%)
0	**Base Mode: No Desorption**		**1947.73**	**0**	**0**
1	500	200	2055.56	107.83	5.54
2	1000	90	2018.07	70.34	3.61
3	520	55	1979.45	31.72	1.63
4	673	115	2023.62	75.89	3.90

Table 4: Effect of desorption on gas recovery in Marcellus Shale

Impact of Proppant Crushing: Presented in **Fig. 27** is conductivity change versus net pressure for 5 different proppant types. Independent labs typically generate the information depicted for various proppant manufactures; the information presented in Fig. 27 is from Santrol Inc. Though the primary object of this work is to assess the performance of Marcellus shale gas reservoirs using 100 mesh sand proppant, for the purpose of comparison, conductivity multipliers have also been provided for 2 types of 40-70 mesh sand, and a resin coated proppant made from a mixture of various mesh sizes size (100 mesh and larger Northern White sand proppant). The data presented in Fig. 27 was incorporated in the numerical simulator to assess the impact that proppant crushing has on

gas production; the results of these simulations are presented in **Fig. 28** and **Fig. 29.**

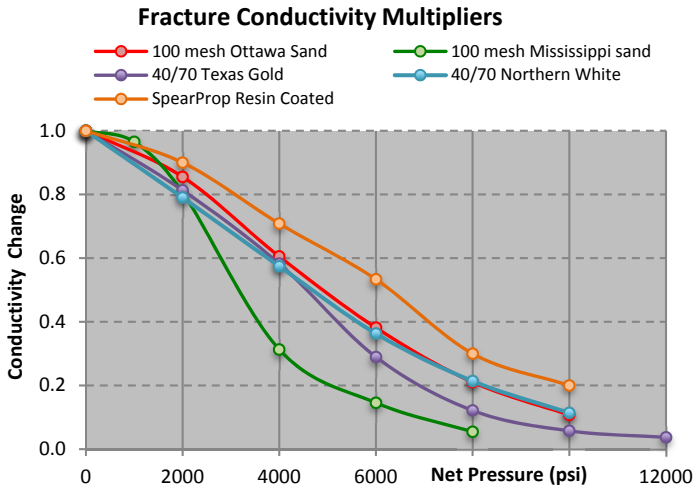

Figure 27: Fracture conductivity change for proppant crushing

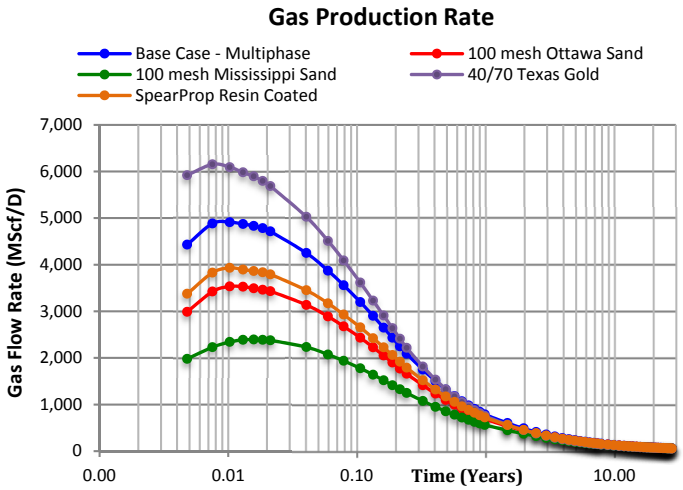

Fig. 28: Gas production rates for various proppants with proppant crushing effects captured

Fig. 27 shows that the smaller 100 mesh proppants tend to maintain conductivity better than 40-70 sand, especially at lower net pressures. However, since 40-70 proppants have a 2 to 3 times larger initial proppant pack conductivity compared to 100 mesh sand, the initial gas flow rate and ultimate recovery are usually higher. Fig. 28 and Fig. 29 also show the superiority of resin-coated proppants over conventional uncoated proppants. On average, the Spearprop resin coated proppant has a smaller diameter than the 40-70 mesh sand, and has an initial proppant pack conductivity 1/3 that of the 40/70 Texas gold sand. However, even though there is great disparity between the initial gas flow rates, the Spearprop resin coated proppant cumulative recovery after 27 years is very similar to that of the 40-70 Texas gold sand. This is evidence of resin coated proppants ability to better withstand crushing when compared to conventional uncoated proppants.

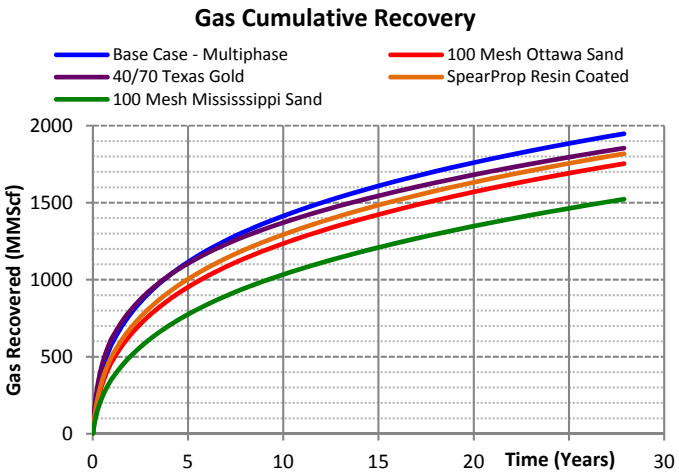

Fig. 29: Cumulative gas recovered for various proppants with proppant crushing effects captured

Comparing the cumulative gas recovered from the base case model that was propped with 100 mesh Ottawa sand (*effects of crushing not modeled*) to that recovered from the model propped with 40-70 Texas gold sand (*effects of crushing included*), we see that the base case model produced 100 MMScf more gas after 27 years (Fig. 29) while having only 1/3 the conductivity of the 40-70 Texas gold proppant. After incorporating the crushing data for 100 mesh Ottawa sand proppant, the simulator predicted that 1753 MMScf of gas will be recovered after 27 years; this is 10 % less than the base model with 100 mesh Ottawa sand (*effects of proppant crushing not modeled*). If 100 mesh Mississippi sand was used instead of 100 mesh Ottawa sand, and we account for proppant crushing, there is a 22% difference in cumulative gas recovered after 27 years compared to the base model. Osholake, Wang et al (2011), used a numerical reservoir simulator to investigate the impact of proppant crushing on a single-phase 160 acre shale gas reservoir. This research investigated the extent to which ceramic and resin coated proppants can be crushed, and the impact this has on fracture conductivity and cumulative gas recovered. Results from this analysis showed, on average, a 6% reduction in the cumulative gas recovered when ceramic and resin coated proppants are used. Figure 29 shows a 6.6% reduction in cumulative gas recovered when SpearProp resin coated proppant is simulated, compared to 10 to 22 percent when sand proppant is used. These results show that proppant type selection is critical for hydraulically fractured Marcellus shale gas reservoirs, and the effects of proppant crushing must be included when attempting to simulate the performance of these reservoirs.

Proppant Diagenesis Effects: Extensive research has been performed by Lee, Elsworth et al (2009) on the impact that diagenesis has on ceramic proppant pack permeability. These results were later incorporated in research works by Osholake, Wang et al (2011); the details of these results are presented in

Fig. 30 as a fracture conductivity change versus time for two types of ceramic proppants.

There are two points that are worthwhile mentioning at this point: the first of which is diagenesis experimental data is available only for the first 1000 days prior to contact of formation rock, proppant, and hydraulic fracture fluids, and no diagenesis data, in the form of a conductivity multiplier, is available for our base model proppant, which is 100 mesh sand. In an attempt to alleviate the first shortcoming, we performed a logarithmic extrapolation of the fracture conductivity multiplier, illustrated by the broken lines in Fig. 30. This extrapolation represents a worse case scenario; we believe that even though diagenesis processes will continue throughout the life of the reservoir, the rate of decline of the proppant pack conductivity will reduce with time, eventually reaching a pseudo steady state where the rate of deposition of minerals on and around individual proppants will be approximately equal to rate at which they are dissolved.

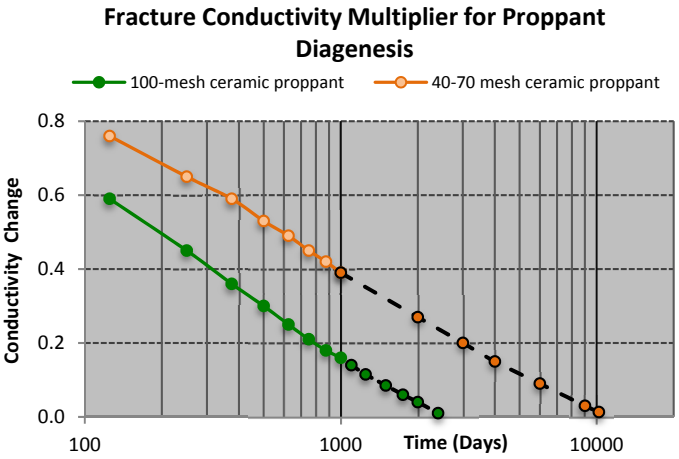

Fig. 30: Fracture conductivity change for proppant diagenesis

Fig. 31 presents a comparison between our base model that uses 100-mesh Ottawa sand and the following four scenarios:

1. Model uses 100-mesh ceramic proppant and diagenesis data included only for the first 1000 days of production (*Model A*).
2. Model uses 100-mesh ceramic proppant and diagenesis data applied to the model includes the extrapolation shown in Figure 30 (*Model B*).
3. Model uses 40-70 ceramic proppant and diagenesis data included for only the first 1000 days of production (*Model C*).
4. Model uses 40-70 ceramic proppant and diagenesis data applied to the model includes the extrapolation shown in Figure 30 (*Model D*).

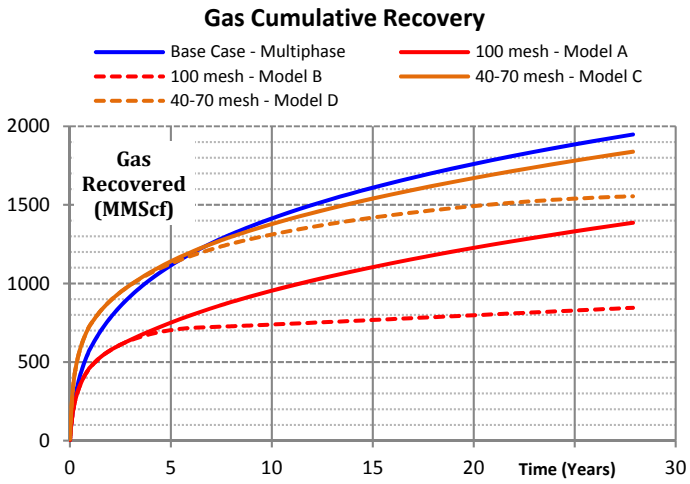

Figure 31: Cumulative gas recovered for ceramic proppants with proppant diagenesis effects captured

Fig. 31 shows that a substantial shortfall in cumulative gas production can be expected due to the effects of proppant diagenesis. Noteworthy is the 40-70 ceramic proppant, which has 3 times the conductivity of our base model 100 mesh Ottawa sand, but still produces 5% less gas after 27 years, when the effects of diagenesis is captured. It is also very likely that the recovery from this model is much less when we consider the extrapolated diagenesis data for this proppant type; the extrapolated data suggest that gas recovery from the 40-70 ceramic proppant can be as low as 1554 MMScf (*Model B*), which is 20% less than that recovered from the base model after 27 years. Furthermore, the effects of proppant diagenesis appear to become more substantial as the proppant diameter decreases. This is expected since the primary effect of diagenesis type reactions is to reduce the porosity of the proppant pack, which in turn reduces the proppant pack permeability. Consequently, in Fig. 31 we see that a 100 mesh ceramic proppant can produce as much as 29% to 56% less gas (compared to our base model) after 27 years when the effects of diagenesis is modeled. Osholake, Wang et al (2011) showed that when proppant diagenesis is simulated on a 20-40 ceramic proppant, the 30-year cumulative gas recovered from a numerically simulated 160 acre shale gas reservoir reduced from 1.5 BCF to 1 BCF (33% reduction). The 30-year cumulative gas recovered further reduced 0.6 BCF (60% reduction) when diagenesis is simulated on a 100 mesh ceramic proppant.

Unlike proppant crushing, the effects of proppant diagenesis require time to manifest. This is demonstrated in **Fig. 32** where very similar early time gas production rates are observed between the base case model and the Models with 100 mesh ceramic proppant (*Models A and B*). The effects of proppant crushing on the other hand takes effect instantaneously after the well is put on production. This behavior is attributed to the fact that some of the proppants are immediately crushed by the created fractures that close on the

proppant pack after fracking is concluded, and the well is shut-in. Consequently, substantial differences in the early time gas production rates are observed between the base case model (*effects of proppant crushing not modeled*) and 100 mesh sand models presented in Fig. 28.

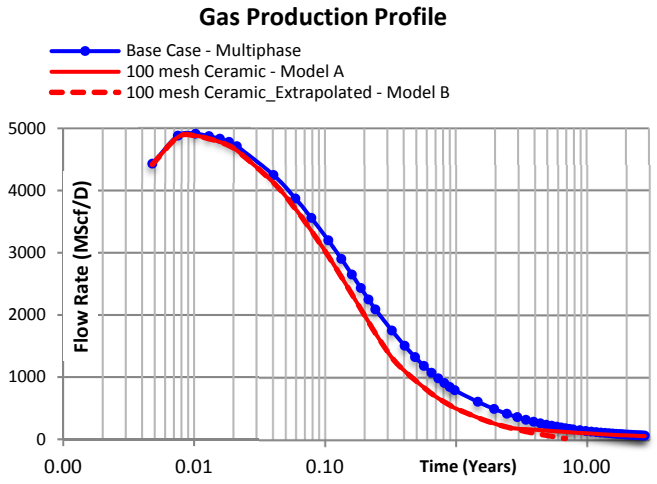

Figure 32: Gas production rates with proppant diagenesis captured

Comparing the effects of proppant diagenesis and proppant crushing, we see that even though proppant crushing has a more substantial impact on early time gas flow rates and cumulative gas recovered (Refer to Fig. 28 & Fig. 29) relative to proppant diagenesis, over the long-term, the effects of proppant diagenesis becomes more pronounced. This is evident in the cumulative gas recovered after 27 years; the effects of proppant crushing can potentially reduce the cumulative gas production by 10% but diagenesis type reactions can reduce cumulative recovery (for a 100 mesh proppant) by 29% or more. These results point to the importance that operators must place on the potential impact that diagenesis type reactions can have on shale gas production.

Impact of Reservoir Rock Compaction: To capture the effect of pore volume reduction (compaction) caused by increasing effective stress during production, we assumed that matrix pore volume compressibility is 3 x 10^{-6} psi^{-1}. Since we did not have any justification for using 3.0E-6 1/psi as the compressibility for the reinitiated natural and created hydraulic fractures, our first compaction simulation assumed that the fractures are rigid (subsequent to initial closure on the proppants) and the only volume that changes due to compaction is the matrix pore volume. The production profile for this simulation, compared to our base model, is presented in **Fig. 33 and Fig. 34.** Whereas reservoir rock compaction is an important recovery mechanism (compaction drive) in conventional oil reservoirs, we see that its impact on shale gas reservoirs is almost negligible. Minor improvements in water and gas production rates were observed during early time production but these increases were not sufficiently substantial to warrant consideration. Although 1st day gas production rate for the simulation that captured matrix pore volume compaction was 13 Mcf higher than our base model (no compaction simulated), table **Table 5** also shows that the cumulative gas recovered after 30 years was only 0.41% (8.12 MMscf) higher than the base case model. Similar observations were made for water recovery, as illustrated in Fig. 34 and Table 5.

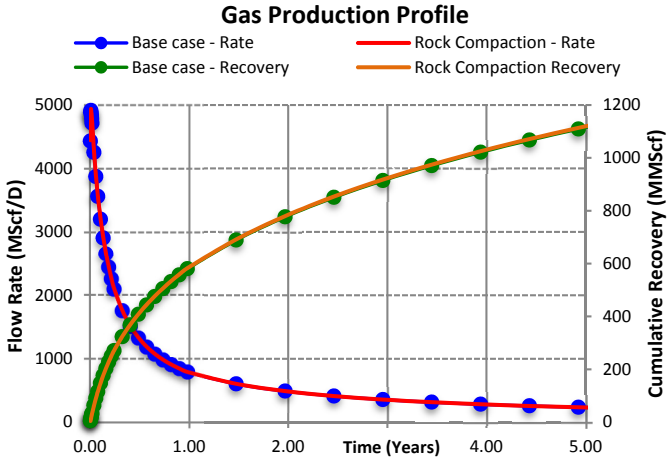

Figure 33: Gas production profile illustrating the effect of reservoir rock compaction

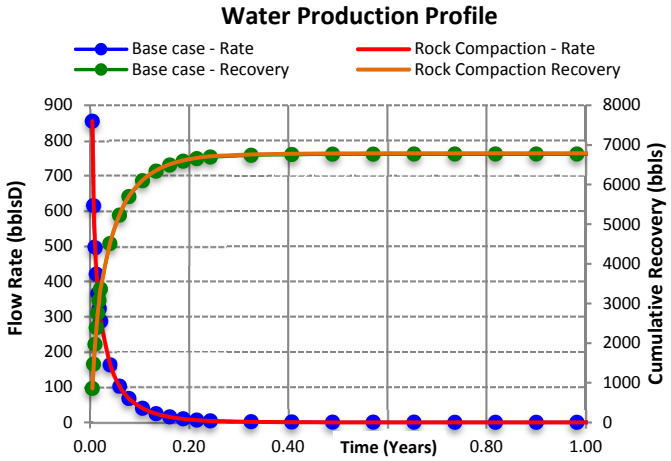

Figure 34: Water production profile illustrating the effect of reservoir rock compaction

Simulation Description	1st Day Recovery Rates				30 years Recovery					
	Gas Recovery (Mscf/D)	Diff. (Mscf)	Water Recovery (bbl/D)	Diff. (bbls)	Gas Recovered (MMscf)	Diff. (MMscf)	% Diff.	Water Recovered (bbls)	Diff. (bbls)	% Diff.
Base Case (No Compaction)	4430.97	0.00	854.15	0.00	1988.37	0.00	0.00	6765.93	0.00	0.00
Matrix Pore Volume Compaction Only	4444.06	13.09	855.09	0.93	1996.50	8.12	0.41	6788.78	22.84	0.34
Matrix Pore and Fracture Volume Compaction	4435.09	4.12	860.22	6.07	1997.59	9.21	0.46	6797.56	31.63	0.47

Table 5: Recovery rates and cumulative recovery as a function of rock compaction

Fig. 33 and Fig. 34 show that gas and water recovery rate and cumulative recovery for the model that included reservoir rock compaction are almost identical to those of our base model (*rock compaction not modeled*); differences are illustrated in Table 5. These very minor improvements in gas production, compared to those observed in conventional oil reservoirs, as it relates to compaction drive, can be attributed to the very low porosity in the shale matrix (3%), the already high relative permeability to gas, and gas high compressibility. Consequently, gradual changes in the shale matrix porosity across each time step does not translate into substantially higher gas production rates.

All reinitiated natural fractures, including the newly created hydraulic fractures, will have different fracture volume compressibility. However, there is no all-encompassing compressibility value for reinitiated J1 or J2 fractures in Marcellus shale. The fracture volume compressibility for these reinitiated natural fractures and the newly created hydraulic fractures is a function of proppant size, proppant compressive strength, proppant concentration, proppant embedment, over burden, other regional stresses, and other factors. Nonetheless, we were also curious about how potential changes in fracture volume will affect recovery from the standpoint of fracture compaction. To address this, we tracked the injected fluid front and applied the same 3.0E-6 1/psi compressibility to all contacted/reinitiated natural fractures, in addition to the created hydraulic fractures; fracture permeability was assumed constant. At the same time, 3.0E-6 1/psi was also applied the rock matrix pore volume. Though a crude approach, this simulation essentially attempted to capture compaction in both the matrix pore volume and fracture volume. Like our previous simulation, which captured pore volume compressibility only, **Fig. 35**, Fig**. 36** and Table 5 shows that fracture volume compaction does not substantially increase either the gas or water recovery rates, when compared to the base case model (no compaction modeled). It is noteworthy that the inclusion of fracture volume compaction increases the 1st day water recovery rate by 6 bbls above the base case model compared to only 0.93 bbls when matrix volume compaction alone is simulated (refer to Table 5). As previous figures showed (Fig.12, Fig. 18 and Fig. 25), the active fractures are almost 100% saturated with water following injection. Therefore, a mechanism such as fracture volume compaction, while reducing the size of the water saturated fractures, will concurrently squeeze water towards the wellbore and thus increase initial water recovery rates.

Failure to see substantial changes in the recovery rates for both gas and water when fracture compaction is simulated (refer to Fig. 35 & Fig. 36) can be explained by the matrix pore volume and fracture volume in the SRV. The total volume of the reinitiated natural fractures and the hydraulic fractures (702,000 cu.ft.) in the SRV is small compared to the matrix pore volume (5,265,000 cu.ft.) in the SRV. Since 3.0E-6 1/psi applied to the matrix pore volume (5,265,000 cu.ft.) has no substantial impact on fluid recovery due to compaction, then applying 3.0E-6 1/psi to the fracture pore volume (702,000 cu.ft.) will also not substantially enhance recovery. If changes in fracture volume are to substantially enhance recovery due to compaction, the fracture volume (total volume of all opened fractures) must be significantly larger and fracture compressibility must be considerably greater than 3.0E-6 1/psi. However, the reader must also be cognizant of the impact that fracture compaction will have on fracture conductivity and in turn gas, and water recovery rates.

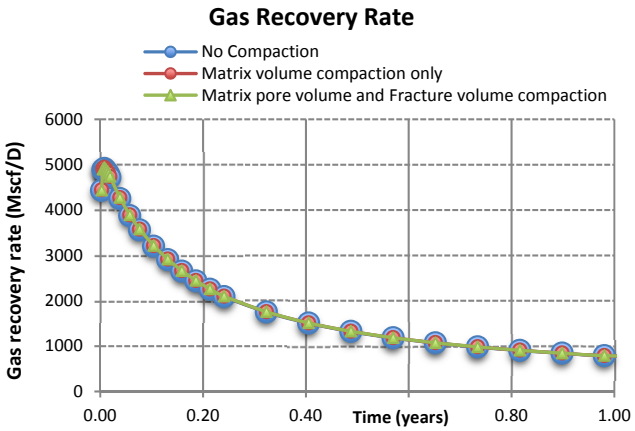

Figure 35: Gas recovery rates as a function of compaction

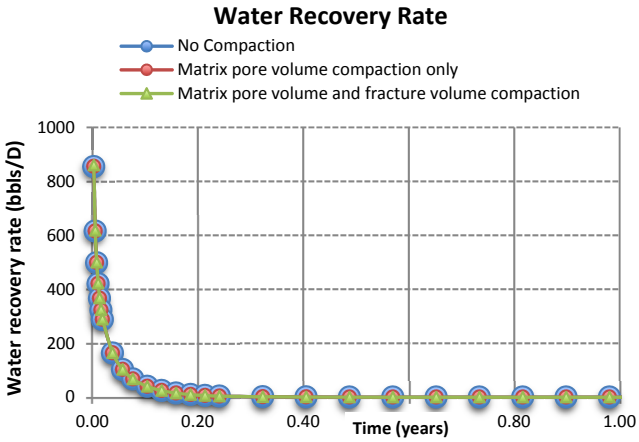

Figure 36: Water recovery rates as a function of compaction

Noteworthy is the potential for a reduction in shale matrix permeability, which accompanies pore pressure depletion during production, and subsequent shale matrix compaction. However, it is our opinion that since shale formations are already extensively compacted, the extent of further compaction triggered by pore pressure depletion will be negligible; this is demonstrated by the insignificant increases in fluid recovery rates presented in this section. Consequently, by extension, we expect that rate reduction caused by changes in permeability, triggered by shale matrix compaction, will also be negligible. Permeability changes caused by shale matrix compaction have not been captured in these simulations. However we anticipate that if such changes are simulated, the negligible increase in fluid recovery rates

caused by compaction will be offset by changes in permeability triggered by pore pressure depletion and subsequent rock compaction. The end result will be an overall null net effect on the system fluid recovery rates and ultimate fluid recovered. Consequently both these phenomena can be ignored when simulation fractured shale gas formation.

Yu and Sepehrnoori (2013) also studied the impact of reservoir rock geomechanics in the Barnett and Marcellus shales, but specifically as it relates to fracture closure stresses and the accompanying fracture conductivity reduction. The authors concluded that rock geomechanics have a negative impact on gas production but this effect becomes less evident as production timelines increase. The authors reported a 4.8% reduction in cumulative gas recovered after 4.5 years of production but this reduces to only 1.8% after 30 years of production. The results suggest that that this aspect of rock geomechanics impacts early time production rates but has a negligible impact on medium and long-term production rates.

Impact of Gas Slippage: Following the work of Ertekin, King et al (1986), a diffusivity coefficient (D_c) of 0.016 sq.f/D, which is based on a matrix permeability of 0.0001mD, was applied to the matrix domain; results are presented **Fig. 37.** Since we suspect variations in the matrix permeability, a sensitivity analysis was performed on the diffusivity coefficient in an attempt to capture this potential variability. The details and results of this analysis are presented in Table 6.

Fig. 37 shows that gas slippage can potentially increase the cumulative gas recovered after 10 years by 7.8%, and by 11% after 27 years of production, when compared to the base case multiphase model (*slippage no captured*). Interestingly, Fig. 37 also shows that when slippage is incorporated in the base case multiphase model, the reservoir produces 73 MMScf (3.5 %) more gas than the single-phase base case model (*slippage not modeled*) after 27 years of production. This shows that gas slippage has a greater positive impact on gas recovery compared to the negative impact multiphase flow has on the same (i.e. reduction in relative permeability to gas flow). Ertekin, King et al (1986), in their work on gas slippage, supported Klinkenberg (1941) conclusion that the gas slippage factor is not constant. They showed that if the dynamic nature of the slippage factor is correctly simulated, gas slippage can account for a 2% to 10% increase in cumulative gas recovered for absolute permeabilities less than 0.01mD.

The results of the sensitivity study **(Table 6)** performed on the diffusivity coefficient (D_c), shows that cumulative gas recovered after 27 years of production does not vary substantially even when Dc is increased by 20%. The Difference column in Table 6 refers to the difference between the original gas recovered and the gas recovered after the diffusivity coefficient is adjusted up or down. A 20% increase in the diffusivity coefficient increases the cumulative gas recovered by only 1.6%, whereas a 20% reduction in D_c reduces the cumulative gas recovered after 27 years by only 1.7%. This shows that the system performance is not noticeably sensitive to the diffusivity coefficient, and therefore minor variations that may exist in the shale matrix permeability may be ignored when one is considering the dynamic gas slippage concept in shale gas reservoirs.

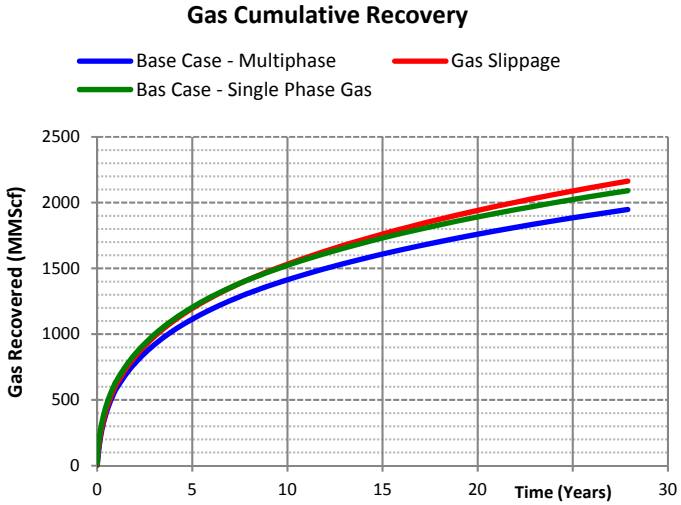

Figure 37: Gas recovery profiles illustrating the impact of dynamic gas slippage

% Change	Dc sq.ft/D	Gas Recovered (MMScf)	Difference (MMScf)	Difference (%)
20%	0.0192	2198.28	34.55	1.60
10%	0.0176	2181.28	17.55	0.81
5%	0.0168	2172.58	8.85	0.41
Original Value	**0.0160**	**2163.73**	**0.00**	**0.00**
-5%	0.0152	2154.74	-8.99	-0.42
-10%	0.0144	2145.59	-18.14	-0.84
-20%	0.0128	2126.83	-36.90	-1.71

Table 6: Diffusivity coefficients and cumulative gas recovered

Injected Fluid Recovery: As is the case with cumulative gas recovered, gas desorption, gas slippage, reservoir rock compaction and proppant crushing, proppant diagenesis also has an impact on the percentage of fractured fluid recovered. Since there is currently no diagenesis laboratory data for 100 mesh sand in the form of a conductivity multiplier, all future discussions in this paper regarding diagenesis assumes that the 100 mesh Ottawa sand used in our base model behaves similar to the 100-mesh ceramic proppant as it relates to diagenesis type reactions. Consequently, their conductivity multipliers will be similar.

Fig. 38 shows that most of the injected fluid that is recovered is captured within the first 20 to 30 days of production. Our base model showed a 12.8% total injected fluid recovery; after the various physical phenomena were applied, ultimate fluid recovery changed as follows:

a) Gas Desorption – 13%

b) Proppant Diagenesis – 12.4%

c) Gas Slippage – 10.4%

d) Proppant Crushing – 9.7%

Though the differences above appear small, when one considers that each well pad has six laterals, and each lateral uses 2.4 to 7.8 millions gallons of injected fluid, a 1% difference in fractured fluid recovered is substantial from the standpoint of treatment and disposal cost to an operator.

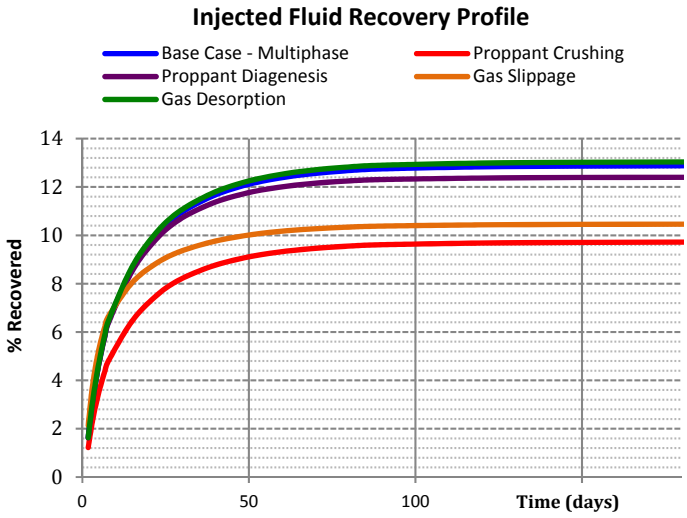

Figure 38: Percentage of Injected Fluid Recovered

Unlike gas recovery, where the impact of proppant diagenesis is more pronounced than the effects of proppant crushing, roles are reverse when we consider the percentage of injected fluid recovered. Since most of the injected fluid is recovered within the first 20 to 30 days of production, any mechanism that does not take effect within this period will have negligible impact on injected fluid recovery. As pointed out earlier, diagenesis type reactions require time to take effect whereas proppants are crushed starting at well shut-in. Therefore, the reduction in fracture conductivity caused by crushed proppants is felt instantaneously when production commences.

Considering we injected 220,000 gallons of fluid in each of the 10 stages present in our model, but on average only 12%, or 26,000 gallons/stage was recovered, the question must be ask: Where is the rest of the water? **Fig. 39** illustrates the fluid saturation profile versus time for the matrix and fracture domain of a single numerical block. We observe that during injection, water saturation in the fractures increased from 0.1 to approximate 1.0; after production commenced, water saturation in the fractures quickly fell off. In the case of the matrix domain, water saturation also quickly increased during injection from 0.1 to 0.15. However, instead of decreasing when production commenced, water saturation in the matrix domain continued to increase to 0.274, and does not fall below 0.27 during the producing life of the model. This behavior is attributed to the high capillary pressures in the matrix that causes water to imbibe into the matrix domain even after production commences. The missing 193,600 gallons of injected fluid per stage is consequently trapped in the matrix domain due to capillary end forces.

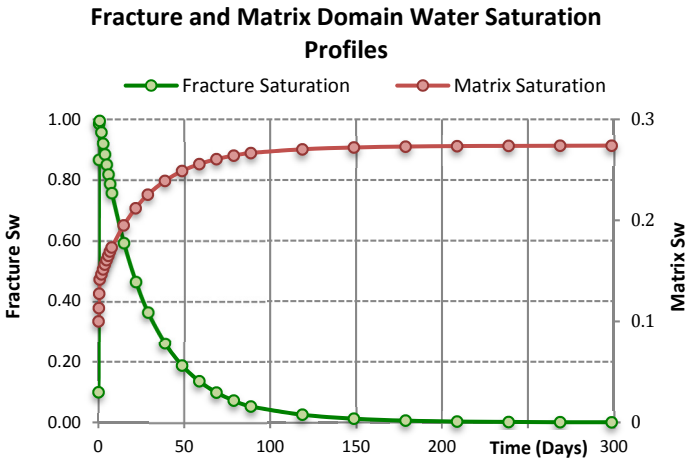

Figure 39: Change in water saturation (%) in the fracture and matrix domain for a single numerical block

Combined Mechanisms: The phenomena discussed above, though initially assessed as individual mechanism with no interrelations among themselves, typically act in tandem in a shale gas reservoir. Gas desorption occurs at the same time that pore volume decreases due to rock compaction, and gas is slipping through the pore throats in the matrix. Additionally, as the foregoing occurs, diagenesis type reactions reduces the permeability of the proppant pack, and increasing effective stress in the hydraulic fractures crush proppants further reducing fracture conductivity. Consequently, to develop a realistic forecast of a shale gas reservoir performance, all these mechanisms must be simultaneously captured within the numerical simulator.

The combination of reservoir rock compaction, dynamic gas slippage, and gas desorption with either the experimental data for proppant crushing or proppant diagenesis poses no problem with data overlap. However, attempting to combine the experimental data for proppant crushing and proppant diagenesis within one numerical simulation poses some potential data conflicts. No information was presented by either referenced source on whether proppant crushing played a role in the proppant pack conductivity reduction observed in the diagenesis experiments. Therefore combining these two data sets can potentially mean that the effects of proppant crushing is duplicated. However, for completeness, the results for such a simulation and several others are presented in **Fig. 40;** summary results are presented in **Table 7.** The Difference column in Table 7 refers to the difference between the original gas recovered from our Base Case multiphase flow and the gas recovered after other damage mechanisms are simulated.

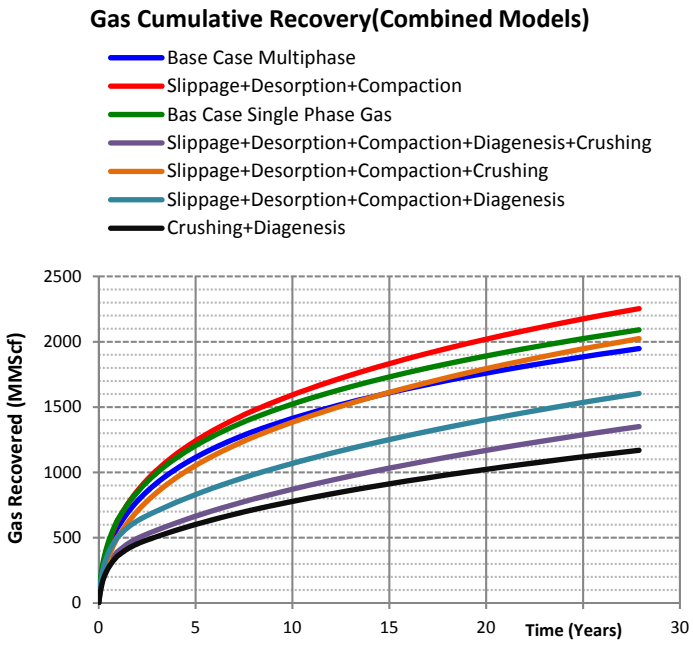

Figure 40: Cumulative gas recovered as a function of various combined mechanisms

SIMULATED MECHANISMS	Gas Recovered (MMScf)	Difference (MMScf)	Difference (%)
Base Case - Single Phase Gas	**2091.11**	**143.38**	**7.36**
Base Case - Multiphase	**1947.73**	**0.00**	**0.00**
Slippage+Desorption+Compaction	2253.42	305.69	15.69
Slippage+Desorption+Compaction + Proppant Crushing	2023.51	75.78	3.89
Slippage+Desorption+Compaction + Proppant Diagenesis	1604.27	-343.46	-17.63
*** Slippage+Desorption+Compaction + Proppant Crushing + Diagenesis	1350.79	-596.94	-30.65
*** Proppant Crushing + Proppant Diagenesis	1169.45	-778.28	-39.96

*** *Possible data overlap between proppant crushing and proppant diagenesis input data*

Table 7: Cumulative gas recovered after 27 years for various simulated mechanisms

Fig. 40 shows that when gas slippage, gas desorption and reservoir rock compaction is considered, cumulative gas recovered after 27 years can be as much as 15% higher (305 MMScf) than the base model. However, if the effects of proppant diagenesis are included, cumulative gas recovered can be reduced by as much as 17%. The addition of proppant crushing to this scenario can further reduce cumulative gas recovered by 13%; total gas recovered will therefore be approximately 30% lower than the base model (*effect of diagenesis and proppant crushing not considered*). Noteworthy is that in absence of proppant diagenesis effects, cumulative gas recovered can be 3.89% higher due to the effects of gas slippage, gas desorption and reservoir rock compaction, even in the present of proppant crushing effects. These results points to the severe detrimental effects that diagenesis type reaction can have on fracture conductivity, especially when smaller mesh size proppants are utilized.

Base on these results, it is evident that operators should give due consideration especially to the potential adverse effects of diagenesis type reactions, but also to the positive impact of gas desorption and gas slippage, and the detrimental effects of proppant crushing, when attempting to develop a realistic forecast for a shale gas reservoir.

Conclusions

The results show that gas slippage, gas desorption, proppant crushing, and proppant diagenesis play a pivotal role in the recovery of shale gas. However, well shut-in time following fracture treatment has a negligible impact on gas recovery. The results also show:

1. The effects of multiphase shale gas recovery, with the associated relative permeability changes this causes, can reduce cumulative gas recovered by 7% during the life of the reservoir.
2. Although longer shut-in times increase fracture fluid leakoff, and substantially reduces the percentage of injected fluid recovered, shut-in time does not severely impact shale gas recovery in the long-term.
3. Gas desorption accounts for a 1.6% to 5.5% of the cumulative gas recovered in Marcellus shale over the producing life of a reservoir.
4. Smaller mesh size sand proppants are more resistant to crushing effects than larger mesh size sand proppants, whose proppant pack conductivity appear to be very susceptible to crushing at low effective stresses. However, since the larger mesh size sand proppants can have an initial conductivity that is as much as 3 times that of smaller sand proppants, initial gas flow rate, and ultimate recovery are usually higher even in the presence of crushing effects.
5. Depending on the proppant type and mesh size selected, proppant-crushing effects can reduce ultimate gas recovery by as much as 10% to 20%.
6. Even though the effects of proppant crushing on early-to-mid term gas recovery is more significant than that of proppant diagenesis, the effects of diagenesis type reaction on long-term gas recovery is much more substantial. Depending on the mesh size selected (smaller mesh sizes being more susceptible), proppant diagenesis can reduce shale gas ultimate recovery by 29% or more.
7. In the absence of permeability changes triggered by pore pressure depletion during production and subsequent matrix compaction, reservoir rock geomechanics (reservoir rock compaction) cause insignificant increases in shale gas recovery rates,

and very minor changes to the percentage of fracture fluid recovered. In the presence of permeability changes, a null net effect on the system recovery rates and ultimate fluid recovery is expected.

8. Dynamic gas slippage can potentially increase the cumulative gas recovered after 10 years by 7.8%, and by 11% after 27 years of production.
9. Gas slippage has a greater positive impact on gas recovery compared to the negative impact multiphase flow has on the same (i.e. reduction in relative permeability to gas flow).
10. System performance is not noticeably sensitive to the diffusivity coefficient, and therefore minor variations that may exist in the shale matrix permeability may be ignored when one is considering the dynamic gas slippage concept in shale gas reservoirs.
11. Between 4% and 15% of the injected fluid will be recovered within the first 50 days of production depending on operation procedures and the impact of the various damage mechanisms. Front end loading of the water treatment and disposal system must be accounted for in the site design and operating procedures.

The reader is reminded that presented results and conclusions are drawn specifically from analysis of a simulated reservoir that captures Marcellus shale gas formation properties. However, we hypothesize that the general trends seen in the results and summarized in the conclusions will also be observed in other shale gas formations. Nonetheless, the reader must be cognizant that no two (2) formations are identical and fields are developed and operated differently. Therefore, some variation in the numbers presented in the results should be expected among different shale gas formations.

DISCLAIMER

This project was funded in part by the Department of Energy, National Energy Technology Laboratory, an agency of the United States Government, through a support contract with URS Energy &Construction, Inc. Neither the United States Government nor any agency thereof, nor any of their employees, nor URS Energy & Construction, Inc., nor any of their employees, makes any warranty, expressed or implied, or assumes any legal liability or responsibility for the accuracy, completeness, or usefulness of any information, apparatus, product, or process disclosed, or represents that its use would not infringe privately owned rights. Reference herein to any specific commercial product, process, or service by trade name, trademark, manufacturer, or otherwise, does not necessarily constitute or imply its endorsement, recommendation, or favoring by the United States Government or any agency thereof. The views and opinions of authors expressed herein do not necessarily state or reflect those of the United States Government or any agency thereof.

Nomenclature

A - Area, ft^2

b - Gas slippage factor

b_a – Apparent gas slippage factor

B_w - Water formation Volume factor, RB/STB

CMBC – Cumulative Mass Balance Check

C_r - Conductivity ratio

c_g - Gas Compressibility, psi^{-1}

D_c - Diffusivitiy coefficient, ft^2/D

IMBC – Incremental Mass Balance Check

k - Absolute permeability, mD

k_f - Fracture permeability

k_r - Relative permeability, mD

L_f - Fracture length, ft

M - phase mobility

m – Time step number

N_x, N_y, N_z – Number of grid blocks in the x, y and z directions

NTS – Not to scale

n – Iteration number

p - Pressure, psi

P_L - Langmuir pressure, psi

p_p - Formation pore pressure, psi

Q^* - Source or sink term for a given phase

q_w - Water flow rate, STB/D

q_{wsc} - Water flow rate at standard conditions, STB/D

q_g - Gas flow rate, Scf/D

S - Saturation, fraction

v - Superficial velocity

v_α^D - Superficial velocity for Darcy type flow for phase α

v_α^s - Superficial slip velocity due to diffusion for phase α

v_α^T - Total superficial velocity for phase α

w_f - Fracture width

V_E - Volume of adsorbed gas per unit volume of reservoir rock, scf/cu.ft

V_L - Langmuir volume, scf/cu.ft

V_b - Bulk Volume, ft^3

z - Gas compressibility factor

Z - Elevation referenced from datum, ft

Greek Symbols

α_c - Volume conversion factor, 5.614583

β - Non-Darcy flow coefficient

β_c - Transmissibility conversion factor, 1.127

β_f - Unit conversion constant, $6.328 \times 10^{-3}\ \frac{\text{sq ft}-\text{cp}}{\text{psi}-\text{md}-\text{day}}$

ρ - Fluid density

μ - Viscosity, cp

ϕ - Porosity, fraction

γ - Phase gravity, psi/ft

σ - Shape factor, sq.ft $^{-1}$

σ_e - Effective stress, psi

σ_{min} - Minimum insitu stress, psi

Other Symbols

∇ - Differential operator

Δ - Gradient operator

Δ_{g_F-Ma} - Gradient operator across the Fracture (F) and Matrix (Ma) domain in the gas (g) phase

Δ_{w_F-Ma} - Gradient operator across the Fracture (F) and Matrix (Ma) domain in the water (w) phase

References

Abah, A. I. (2013). Effect of multi-phase flow on recovery of fracture fluid and gas in Marcellus Shale reservoirs. Dissertation/Thesis, Pennsylvania State University.

Blauch, M. E., Myers, R. R. et al. (2009). Marcellus Shale Post-Frac Flowback Waters - Where is All the Salt Coming from and What are the Implications? Presented at the SPE Eastern Regional Meeting, 23-25 September, Charleston, West Virginia. SPE-125740-MS.

Boulis, A., Jayakumar, R. et al. (2012). Improved Methodologies for More Accurate Shale Gas Assessments. Presented at the SPE SPE Americas Unconventional Resources Conference, 5-7 June, Pittsburgh, Pennsylvania. SPE-154981-MS.

Charoenwongsa, S., Kazemi, H. et al. (2013). Simulation of Gel Filter-Cake Formation, Gel Cleanup, and Post-Fracture Well Performance in Hydraulically Fractured Gas Wells. *SPE Production & Operations* 28, (03): 235-245. SPE-150104-PA.

Chawathé A. (1995). Development and testing of a dual-porosity, dual-permeability simulator to study multimechanistic flow through tight, fractured reservoirs. Dissertation/Thesis, Pennsylvania State University.

Chawathé, A., Ertekin, T. et al. (1996). Numerical Simulation of Multimechanistic Gas-Water Flow in Fractured Reservoirs. Presented at the Permian Basin Oil and Gas Recovery Conference, 27-29 March, Midland, Texas. SPE-35186-MS

Cikes, M. (2000). Long-Term Hydraulic-Fracture Conductivities Under Extreme Conditions. *SPEPF* 15 (4): 255–261. SPE-66549-PA.

Cinco L, H., Samaniego V, F. et al. (1978). Transient Pressure Behavior for a Well With a Finite-Conductivity Vertical Fracture. *SPE Journal*, 18 (04): 253-264. SPE-6014-PA.

Cinco-Ley, H. and Samaniego V, F. (1981). Transient Pressure Analysis for Fractured Wells. *Journal of petroleum technology*, *33*(09): 1-749. SPE-7490-PA.

Cipolla, C. L., London E. P., et al. (2010). Reservoir Modeling in Shale-Gas Reservoirs. *SPE Reservoir Evaluation & Engineering. 13*(04): 638-653. SPE-125530-PA.

Clarkson, C. R., Nobakht, M. et al. (2012). Production Analysis of Tight-Gas and Shale-Gas Reservoirs Using the Dynamic-Slippage Concept. *SPE Journal* 17(01): 230-242. SPE-144317-PA.

Coles, M. E. and Hartman, K. J. (1998). Non-Darcy Measurements in Dry Core and the Effect of Immobile Liquid. Presented at SPE Gas Technology Symposium, 15-18 March, Calgary, Alberta. SPE-39977-MS.

Cooke, C. E., Jr. (1973). Conductivity of Fracture Proppants in Multiple Layers. *Journal of Petroleum Technology*, *25*(09): 1-101. SPE-4117-PA

Dickins, M., McVay, D. et al. (2008). The Impact of Gravity Segregation on Multiphase Non Darcy Flow in Hydraulically Fractured Gas Wells. Presented at the SPE Annual Technical Conference and Exhibition, 21-24 September, Denver, Colorado. SPE-116748-MS.

Ertekin, T., King, G. A. et al. (1986). Dynamic Gas Slippage: A Unique Dual-Mechanism Approach to the Flow of

Gas in Tight Formations. *SPE Formation Evaluation* 1(01): 43-52. SPE-12045-PA.

Evans, R. D., Hudson, C. S. et al. (1987). The Effect of an Immobile Liquid Saturation on the Non-Darcy Flow Coefficient in Porous Media. *SPE Production Engineering*, *2*(04): 331-338. SPE-14206-PA.

Fathi, E. and Akkutlu I. Y. (2012). Mass Transport of Adsorbed-Phase in Stochastic Porous Medium with Fluctuating Porosity Field and Nonlinear Gas Adsorption Kinetics. *Transport in porous media* 91(1): 5-33.

Frederick, D. C., Jr. and Graves R. M. (1984). New Correlations To Predict Non-Darcy Flow Coefficients at Immobile and Mobile Water Saturation. Presented at the SPE Annual Technical Conference and Exhibition, 25-28 September, New Orleans. SPE-28451-MS.

Gao, C., Lee, W. J. et al. (1994). Modeling Multilayer Gas Reservoirs Including Sorption Effects. Presented at the SPE Eastern Regional Meeting, 8-10 November, Charleston, West Virginia. SPE-29173-MS.

Gdanski, R. D., Fulton, D. D. et al. (2009). Fracture-Face-Skin Evolution During Cleanup. *SPE Production & Operations* 24(01): 22-34. SPE-101083-PA.

Gdanski, R. D., Weaver, J. D. et al. (2007). A New Model for Matching Fracturing Fluid Flowback Composition. Presented at the SPE Hydraulic Fracturing Technology Conference, 29-31 January, College Station, Texas. SPE-106040-MS.

Gdanski, R. D., Weaver, J. D. et al. (2005). Fracture Face Damage—It Matters. Presented at the SPE European Formation Damage Conference, 25-27 May, Sheveningen, The Netherlands. SPE-94649-MS.

Geertsma, J. (1974). Estimating the Coefficient of Inertial Resistance in Fluid Flow Through Porous Media. *SPE Journal*, *14*(05): 445-450. SPE-4706-PA.

Gewers, C. W. W. and Nichol L. R. (1969). Gas Turbulence Factor in a Microvugular Carbonate. *Journal of Canadian Petroleum Technology, 8(02): 51-36.* PETSOC-69-02-02.

Godec, M., Koperna, G. et al. (2013). Potential for enhanced gas recovery and CO_2 storage in the Marcellus Shale in the Eastern United States. *International Journal of Coal Geology* 118(0): 95-104.

Halliburton (2009). Meeting the Challenges of the Marcellus Shale Through Technology.

Han, J., Wang, J. Y. et al. (2014). A Fully Coupled Geomechanics and Fluid Flow Model for Proppant Pack Failure and Fracture Conductivity Damage Analysis. Presented at the SPE Hydraulic Fracturing Technology Conference, 4-6 February, The Woodlands, Texas. SPE-168617-MS.

Holditch, S. (1979). Factors affecting water blocking and gas flow from hydraulically fractured gas wells. *Journal of Petroleum Technology* 31(12): 1515-1524. SPE-7561-PA.

Janicek, J. D. and Katz D. L. V. (1955). Applications of unsteady state gas flow calculations.

Jones, S. (1987). Using the inertial coefficient, b, to characterize heterogeneity in reservoir rock. Presented at the SPE Annual Technical Conference and Exhibition, 27-30 September, Dallas, Texas. SPE-16949-MS.

Katz, D. L. , Cornell, D., Kobayashi, R., Poettmann, R.H., Vary, J.A., Elenbaas, J.R., and Weinaug, C.F. (1959). Handbook of natural gas engineering, McGraw-Hill Book Co. Inc., New York City.

King, G. (1985). Numerical simulation of the simultaneous flow of methane and water through dual porosity coal seams during the degasification process. Dissertation/Thesis, Pennsylvania State University.

Klinkenberg, L. J. (1941). The Permeability Of Porous Media to Liquids And Gases. American Petroleum Institute.

Lee, D. S., Elsworth, D. et al. (2009). An Evaluation of the Effects of Fracture Diagenesis On Fracture Treatments: Modeled Response. Presented at the 43rd US Rock Mechanics Symposium & 4th US-Canada Rock Mechanics Symposium, 28 June-1 July, Asheville, North Carolina. ARMA-09-104.

Li, D., Svec, R. K. et al. (2001). Modeling and Simulation of the Wafer Non-Darcy Flow Experiments. Presented at the SPE Western Regional Meeting, 26-30 March, Bakersfield, California. SPE-68822-MS.

Ning, X., Marcinew, R. et al. (1995). The Impact of Fracturing-fluid Cleanup And Fracture-face Damage On Gas Production. Presented at the Petroleum Society of Canada Annual Technical Meeting, June 7 - 9, Calgary, Alberta. PETSOC-95-43.

Noman, R., Shrimanker, N. et al. (1985). Estimation of the Coefficient of Inertial Resistance in High-Rate Gas Wells. Presented at the SPE Annual Technical Conference and Exhibition, 22-26 September, Las Vegas, Nevada. SPE-14207-MS.

Osholake, T. A., Wang, J. Y. et al. (2011). Factors Affecting Hydraulically Fractured Well Performances in the Marcellus Shale Gas Reservoirs. *Journal of Energy Resources Technology*, *135*(1), 013402.

Palisch, T. T., Duenckel, R. J. et al. (2007). Determining Realistic Fracture Conductivity and Understanding its Impact on Well Performance - Theory and Field

Examples. Presented at the SPE Hydraulic Fracturing Technology Conference, 29-31 January, College Station, Texas. SPE-106301-MS.

Penny, G. S. and Jin L. (1995). The Development of Laboratory Correlations Showing the Impact of Multiphase Flow, Fluid, and Proppant Selection Upon Gas Well Productivity. Presented ath the SPE Annual Technical Conference and Exhibition, 22-25 October, Dallas, Texas. SPE-30494-MS.

Prats, M. (1961). Effect of Vertical Fractures on Reservoir Behavior-Incompressible Fluid Case. *Society of Petroleum Engineers Journal*, *1*(02): 105-118. SPE-1575-G.

Reyes, L. and Osisanya S. O. (2002). Empirical Correlation of Effective Stress Dependent Shale Rock Properties. *Journal of Canadian Petroleum Technology*. PETSOC-02-12-02.

Schutjens, P. M. T. M., Hanssen, T. H. et al. (2001). Compaction-Induced Porosity/Permeability Reduction In Sandstone Reservoirs. Presented at the *SPE* Annual Technical Conference and Exhibition, 30 September-3 October, New Orleans, Louisiana. SPE-71337-MS.

Sherman, J. and Holditch, S. (1991). Effect of injected fracture fluids and operating procedures on ultimate gas recovery. P*resented at the SPE Gas Technology Symposium, 22-24 January, Houston, Texas. SPE-21496-MS.*

Tao, Q., Ehlig-Economides, C. A. et al. (2009). Investigation of Stress-Dependent Permeability in Naturally Fractured Reservoirs Using a Fully Coupled Poroelastic Displacement Discontinuity Model. Presented at the SPE Annual Technical Conference and Exhibition, 4-7 October, New Orleans, Louisiana. SPE-124745-MS.

Tek, M. R., Coats, K. H. et al. (1962). The Effect of Turbulence on Flow of Natural Gas Through Porous Reservoirs. *Journal of Petroleum Technology*, *14* (07): 799-806. SPE-147-PA.

Voneiff, G., Robinson, B. et al. (1996). The effects of unbroken fracture fluid on gas well performance. *SPE Production & Facilities*, *11*(04): 223-229. SPE-26664-PA.

Wang, J., Holditch, S. et al. (2010). Modeling Fracture-Fluid Cleanup in Tight-Gas Wells. *SPE Journal* 15(03): 783-793. SPE-119624-PA.

Wang, Y., Holditch, S. A. et al. (2008). Simulation of Gel Damage on Fracture Fluid Cleanup and Long-Term Recovery in Tight Gas Reservoirs. Presented at the SPE Eastern Regional/AAPG Eastern Section Joint Meeting, 11-15 October, Pittsburgh, Pennsylvania. SPE-117444-MS

Weaver, J. D., Nguyen, P. D. et al. (2005). Sustaining Fracture Conductivity. Presented at the SPE European Formation Damage Conference, 25-27 May, Sheveningen, The Netherlands. SPE-94666-MS.

Weaver, J. D., Parker, M. et al. (2007). Fracture-Related Diagenesis May Impact Conductivity. *SPE Journal*, *12*(03): 272-281. SPE-98236-PA.

Wong, S. W. (1970). Effect of Liquid Saturation On Turbulence Factors For Gas-Liquid Systems. Journal of Canadian Petroleum Technology, 9(04). PETSOC-70-04-08.

Yu, W. and Sepehrnoori, K. (2013). Simulation of Gas Desorption and Geomechanics Effects for Unconventional Gas Reservoirs. Presented at the SPE Western Regional & AAPG Pacific Section Meeting 2013 Joint Technical Conference, 19-25 April, Monterey, California. SPE-165377-MS.

Appendix

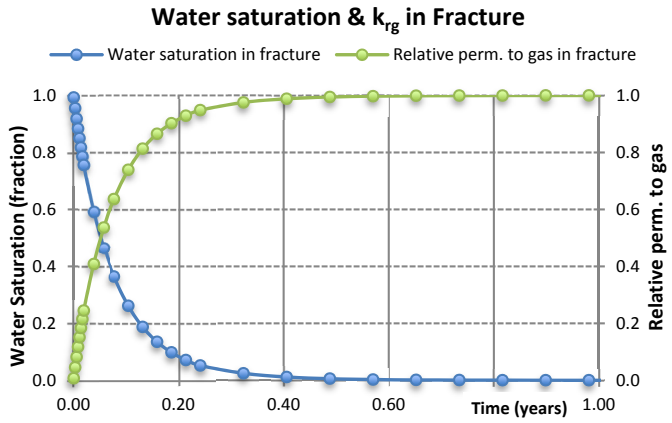

Fig. A1: Changes in relative permeability to gas (k_{rg}) in relation to changes in water saturation (S_w) in a fracture

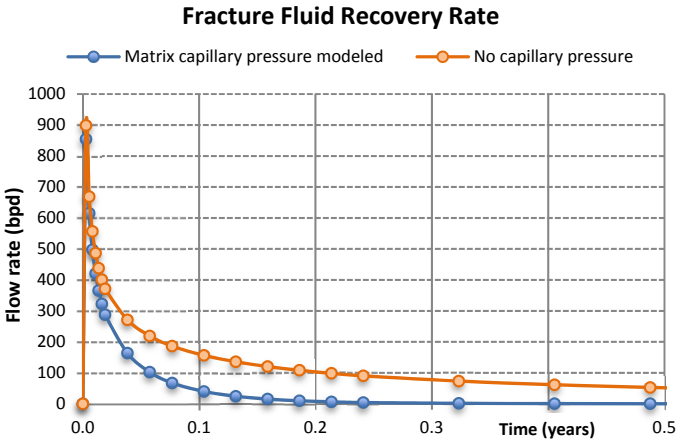

Fig. A2: Impact of matrix capillary pressure on fracture fluid recovery rate

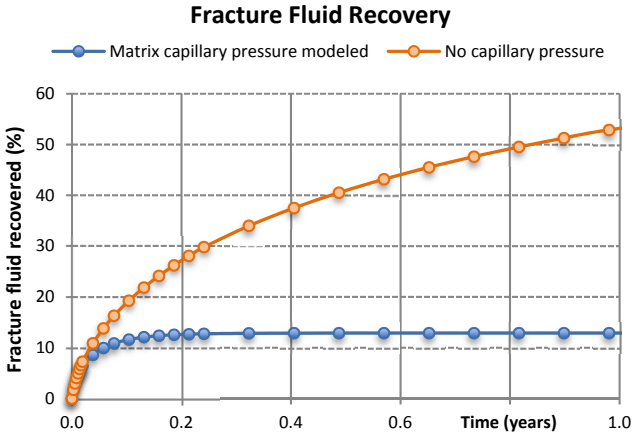

Fig. A3: Impact of matrix capillary pressure on fracture fluid recovery

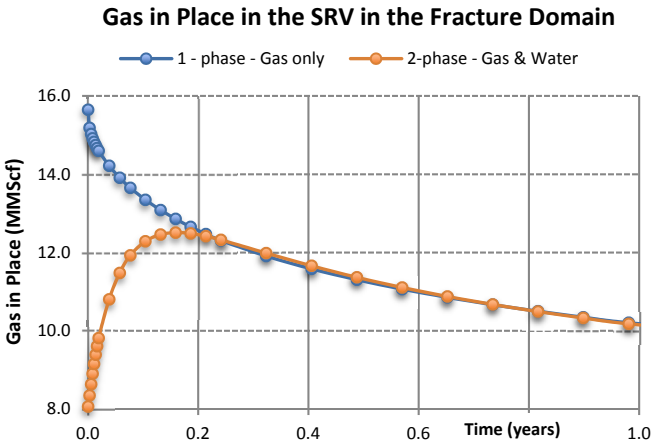

Fig. A4: Gas in place in the fractures of SRV during production